U.PORTO

FEUP FACULDADE DE ENGENHARIA UNIVERSIDADE DO PORTO

AUTOMATED MODAL ANALYSIS FOR MONITORING OF WIND TURBINES

SUSANA GOMES DIAS

Dissertation submitted for partial fulfilment of the requirements for the degree of
MASTER SCIENCE DEGREE IN CIVIL ENGINEERING

SPECIALIZATION IN STRUCTURES AND GEOTECHNICS

Supervisor: Professor Filipe Manuel Rodrigues Leite Magalhães

Co-supervisor: Doctor Sérgio Bouça Pereira

Coordinator at Siemens: Engineer André Guilherme Massano Tavares

JUNE 2024

MASTER IN CIVIL ENGINEERING 2023/2024

CIVIL ENGINEERING DEPARTMENT

Tel. +351-22-508 1901

✉ m.ec@fe.up.pt

Edited by

FACULTY OF ENGINEERING OF UNIVERSITY OF PORTO

Rua Dr. Roberto Frias

4200-465 PORTO

Portugal

Tel. +351-22-508 1400

✉ feup@fe.up.pt

http://www.fe.up.pt

To my family,

The greater our knowledge increases the more our ignorance unfolds.

- John F. Kennedy

AKNOWLEDGMENTS

All my achievements, both personally and in academics, are the result of the knowledge and experiences I've gained with the help of many people, to whom I want to thank sincerely for their support.

I would like to start by thanking Faculty of Engineering of University of Porto and Siemens Digital Industries Software, Belgium, for giving me the opportunity to be a part of this thesis project. I'm especially grateful to my supervisor Professor Filipe Magalhães, to my co-supervisor Doctor Sérgio Pereira and to my coordinator at Siemens Engineer André Tavares for sparking my interest with structural dynamics and wind turbines. I am extremely thankful for their guidance, support, patience, and assistance throughout the thesis project, since their insights were crucial to the success of my research.

Additionally, I want to express my gratitude to the people who journeyed alongside me during this international adventure. Although we began as colleagues, our bonds evolved into friendships, enriching our time together with laughter and camaraderie. Thank you for transforming this unexpected semester in Belgium into a place of warmth and belonging, overflowing with cherished memories.

To my dear friends from FEUP, who have accompanied me throughout my academic journey, I owe immense gratitude. Together, we weathered challenging times, and it was your joy, compassion, and understanding that lightened even the darkest moments. Without your support, completing my studies smiling would have been impossible. To all the remarkable people I had the privilege of meeting during my IACES journey, summer internships, and volunteering programs. Your kindness and the lessons you imparted have left an unforgettable mark on me. And to my high school friends, who have witnessed my growth over the years, I am truly thankful for our friendship.

Most importantly, I want to thank my parents, Sandra and Armando, for everything I could build over my life. All their love, unconditional encouragement and efforts were daily felt and a great basis for who I am, alongside with the provided education and opportunities. To my sister, Filipa, my companion throughout our 21 years together.

ABSTRACT

Wind turbines are dynamic structures subject to extreme loads and highly variable environmental conditions. In order to guarantee their structural integrity and consequent longevity, it is imperative to understand their behaviour and, for this reason, various structural monitoring techniques have been developed.

Within the scope of this thesis, the method of automatic operational modal analysis is applied, since its use is relevant to the characterization of structures. Its automation reduces the need for intervention by technicians during the process, reducing the susceptibility to errors and enhancing its application for monitoring over long periods of time.

The method explored consists of three phases: first, PolyMAX is used to identify the modal parameters in each data set, then the modal parameters are automatically selected and the structural modes are tracked, namely the natural frequencies and modal shapes over the course of a year.

The automatic modal parameter selection approach is improved, consisting of DBSCAN (automatic mode aggregation algorithm) and two additional verification steps, with the aim of improving the selection of pole clusters in the stabilization diagrams. In the final stage, the modes are tracked using two approaches: with a single reference and with an adaptive reference depending on the data collected, organized according to the speed of rotation of the wind turbine rotor.

KEYWORDS: WIND TURBINES, AUTOMATIC MODAL ANALYSIS, POLYMAX, DBSCAN, MODAL TRACKING.

RESUMO

As turbinas eólicas são estruturas dinâmicas sujeitas a cargas extremas e a condições ambientais altamente variáveis. Para garantir a sua integridade estrutural e consequente longevidade é imperativo a compreensão do seu comportamento e, por isso, têm sido desenvolvidas diversas técnicas de monitorização estrutural.

No âmbito desta tese, aplica-se o método da análise modal operacional automática, uma vez que a sua utilização é relevante para a caracterização de estruturas e, a sua automatização, permite reduzir a necessidade de intervenção por parte de técnicos durante o processo reduzindo a susceptibilidade a erros e potencializando a sua aplicação para monitorização durante longos períodos de tempo.

O método explorado é composto por três fases: primeiramente, utiliza-se o Polymax para identificação dos parâmetros modais em cada conjunto de dados, de seguida, selecionam-se automaticamente os parâmetro modais e procede-se ao *tracking* dos modos estruturais, nomeadamente das frequências naturais e das formas modais ao longo de um ano.

A abordagem de seleção automática de parâmetros modais é melhorada. Esta é composta pelo DBSCAN (algoritmo automático de agregação dos modos) e por dois passos adicionais de verificação, com o objetivo de aprimorar a seleção dos agrupamentos de polos nos diagramas de estabilização. Numa última fase, procede-se ao *tracking* dos modos utilizando duas abordagens: com uma referência única e com uma referência adaptativa em função dos dados recolhidos organizados consoante a velocidade de rotação do rotor da turbina eólica.

PALAVRAS-CHAVE: TURBINAS EÓLICAS, ANÁLISE MODAL AUTOMÁTICA, POLYMAX, DBSCAN, TRACKING MODAL.

CONTENTS

LIST OF FIGURES

LIST OF TABLES

Symbols, Acronyms & Abbreviations

Symbols

% – Percent Sign

$\overline{S_x}$ – Signal Delayed Complex Conjugate

$\overline{S_y}$ – Complex Conjugate of the Reference Signal

$\cdot^*$ – Complex Conjugate Operator

$\cdot^H$ – Complex Conjugate Transpose (Hermitian) Operator

$\cdot^T$ – Transpose Operator

Ω_r – Polynomial Basis Functions

N_p – Number of Points

S_x – Signal

S_{yy} – Auto And Cross Power Spectral Density Matrix

$S_{yy}^{+}(\omega)$ – Half Spectrum Matrix

g_k – Operational Reference Factors

n_2 – Number of Modes

α_r – Denominator Matrix Polynomial Coefficients

β_r – Nominator Matrix Polynomial Coefficients

± – More or Less

Δt – Sampling Period

° – Degrees

°C – Celsius Degrees

dB – Decibel

g – Grams

GW – Gigawatt

Hz – Hertz

kW – Kilowatts

L – Modal Participation Factor Matrix

m/s – Meters Per Second

MW – Megawatts

rpm – Revolutions per Minute

TWh – Terawatt-hour

Λ – System Poles Diagonal Matrix

Ω – Rotational Frequency of the Rotor

$A(\omega)$ – Denominator Matrix

$B(\omega)$ – Nominator Matrix

$H(\omega)$ – Transfer Function Matrix

LR – Lower Residues

UR – Upper Residues

V – Modal Vector Matrix

f – Frequency

p – Modal Order

γ – System Poles Vector (Modal Participation Factors)

ε – Radius (considered in DBSCAN)

λ – System Poles

ξ – Damping Ratio

φ – Column Vector Containing n_2 Components Of A Certain Mode Shape

ω – Circular Frequency

ϕ – Eigenvector

Acronyms

ACF – Autocorrelation Functions

AMA – Automated Modal Analysis

AMPS – Automated Modal Parameter Selection

AMT – Automated Modal Tracking

ANPSD – Averaged Normalized Power Spectral Density

AOMA – Automated Operational Modal Analysis

APSD – Auto-Power Spectral Densities

CCF – Cross-Correlation Functions

CPSD – Cross-Power Spectral Densities

DBSCAN - Density-Based Spatial Clustering of Applications With Noise

DC – Digital Converter

DFT – Discrete Fourier Transform

EU – European Union

MAC – Modal Assurance Criterion

MPE – Modal Parameter Estimation

OMA – Operational Modal Analysis

P-LSCFD – Poly-Reference Least Squares Complex Frequency Domain Method Or Polymax

PSD – Power Spectral Density Functions

SCADA – Supervisory Control and Data Acquisition

SHM – Structural Health Monitoring

SSI-COV – Covariance Driven Stochastic Subspace Identification Algorithm

SSI-DATA – DATA-Driven Stochastic Subspace Identification Method

UK – United Kingdom

WT – Wind Turbine

Abbreviations

DOF – Degrees-of-freedom

FA – Fore-aft

$minpts$ – Minimum Number of Points

n_prev – Number of Previous Points

PolyMAX– Poly-Reference Least Squares Complex Frequency Domain Method (P-LSCFD)

rp – Representative Poles

SS – Side-side

1
INTRODUCTION

1.1. MOTIVATION

In *COP28*, 133 governments agreed in triple the capacity of renewable energy globally to 11 000GW by 2030 and in enhance energy efficiency improvements to over 4% every year [1]. These objectives were proposed to meet the 1.5 °C limit to temperature increase compared to pre-industrial levels, defined in the *2015 Paris Agreement* [2]. During 2023, 117 GW of new wind power were installed globally and is expected an average grow of 158 GW per year until 2028 [3].

In 2023, Europe (EU-27 and the UK) installed 18.3 GW of new wind capacity, totalizing an installed wind power capacity of 272 GW, being 87.5% onshore. 466 TWh of EU-27 electricity demand was met by wind energy during the same year, representing 19% of the total demand [4]. The *European Wind Power Action Plan* sets the renewable energies should represent 42.5% by 2030 [5] and Portugal's objective, set in *National Energy Plan And Climate 2023*, is to produce 85% of the energy consumption from renewable sources by 2030 and to install 12.4 GW of wind power capacity by then [6, 7].

In 2023, 72.8% electricity production in Portugal was from renewable energy sources, and 40.5% of those are from wind sources [8]. During this year, 61% of the energy consumption was produced by renewable sources and 25% was wind power supplied, corresponding to 12.8 TWh [9].

The constant and consistent wind energy sector growth, represented in Figure 1, and the global investments projected for the coming years indicate an enhancement of challenges related to the operation and maintenance of the wind turbines (WT). Therefore, their monitoring combined with data analysis is decisive to decision making regarding more efficiency and less cost during their life cycle [3]. In this context, Operational Modal Analysis (OMA) has a fundamental role in structures' dynamic characterization.

The OMA process utilizes data collected during the normal operation of the structure, influenced by ambient and operational excitations such as wind, temperature, and blade rotation, all of which are recorded by the SCADA system. For wind turbines, correlating the vibration data with SCADA data is crucial for a comprehensive understanding of their structural dynamics, as these dynamics are significantly affected by operational conditions [10].

The OMA main benefits are its applicability to continuous long-term monitoring of large structures, without imposing artificial excitation; the possibility to estimate modal properties for real operating conditions that can be used in Structural Health Monitoring methodologies [11].

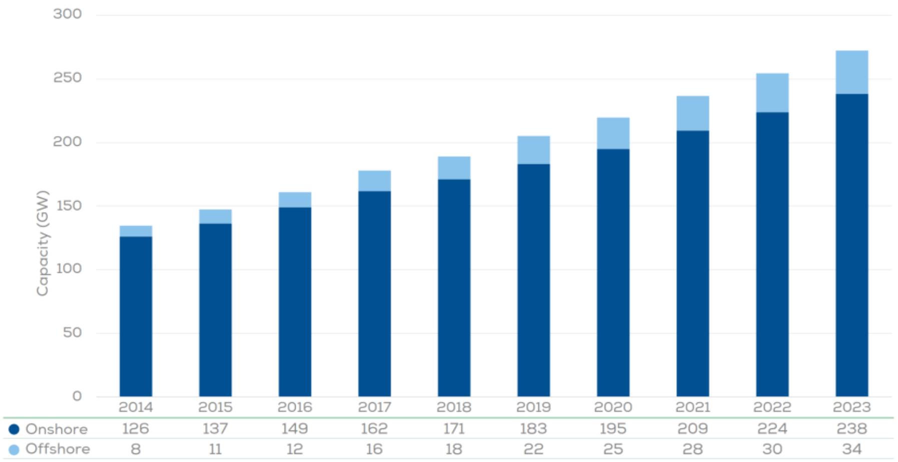

Figure 1 - Annual growth of onshore and offshore wind power capacity installed in Europe [4].

The understanding of wind turbines structural dynamics allows to identify possible behaviour modifications associated with damage or mal functioning, enabling the improvement of predictive maintenance based on usage and real-time characterization. The consequence of operational and environmental conditions should be identified and removed from the modal parameters to reach only the structural effects [12].

Introducing the automated analysis of OMA results is fundamental to reduce analyst errors likelihood, to enhance results repeatability to do long-term monitoring campaigns. Nowadays, Automated Operational Modal Analysis (AOMA) algorithms are commercialized, therefore, their study is relevant to produce improvements and fasten the data analysis [13] [14].

Therefore, in this work an AOMA methodology was further developed and implemented in a one-year data measurements from an onshore wind turbine.

1.2. State-of-the-art

The modal parameters (natural frequencies, mode shapes, and damping ratios) extraction from data recorded is a process that often anticipates vibration-based Structural Health Monitoring (SHM) procedures. An automatic procedure to select the stabilization diagram poles is fundamental to automatize the process and ease its implementation over a wider number of structures, while reducing the susceptibility to errors performed by analysts [15, 16].

Automated Modal Analysis (AMA) is a sequence of three main steps that enables an autonomous analysis of the stabilization diagrams for multiple measurements with repeatability. The first step is the Modal Parameter Estimation (MPE), followed by the Automated Modal Parameter Selection (AMPS) where the modal parameters are automatically selected from the stabilization diagram and, lastly, the Automated Modal Tracking (AMT), whose results enable the modal parameter monitoring along time [14].

The MPE employed in the current work is the poly-reference Least Squares Complex Frequency Domain method (p-LSCFD, also denominated PolyMAX) [17], a frequency-domain methodology. The Covariance driven Stochastic Subspace Identification algorithm (SSI-COV) [18] and the DATA-driven Stochastic Subspace Identification method (SSI-DATA) [19] are time-domain parametric algorithms often used in MPE stage, especially in in the civil engineering field. A review of these algorithms and an introduction to others is presented by Peeters and De Roeck in [18].

Oliveira used the algorithms SSI-COV and p-LSCF to perform AOMA for two onshore wind turbines, using one-year measurement data, and concluded both methods could accurately identify the main vibration modes [20].

The methodologies used to perform AMPS include clustering techniques to associate the poles with similar modal characteristics and the posterior definition of each mode's representative pole. The clustering algorithms can be divided in three main categories: hierarchical [21] [22], density-based [14] [23] [24] and partitioning methods [12] [25] [26] [27].

Dederichs et al. [28] compared four clustering algorithms, validated in different bridge applications, using experimental data from Hardanger Bridge (hierarchical clustering [21]; Hierarchical clustering step, followed by k-means to select final physical clusters [25], *fuzzy C-means clustering* to separate the unstable poles [26]; hierarchical density-based spatial clustering of applications with noise (HDBSCAN) [24]). It was concluded fully automated clustering algorithms have lower consistency but are less prone to errors, when compared to ones that require some user interaction and parameter adjustment.

In the AOMA wind turbine domain, Devriendt used *fuzzy clustering* to analyse datasets from an offshore wind turbine, requiring the previous definition of cluster number [12] and Oliveira monitored an onshore WT during an year resorting in hierarchical clustering [29]. DBSCAN clustering was applied in this context by Teng [23], to clear the stabilization diagram.

The AMT is the last step to perform AMA and it is fundamental to identify the evolution of modal parameters over time and over different operational and environmental conditions [29].

This final stage can be executed by monitoring one or more modal parameters. This method was applied by tracking only the frequency in a masonry tower [30] and an arch bridge during both construction and operational phases [23]. Additionally, Oliveira monitored the evolution of an onshore wind turbine modal parameters, over one year, restricting frequency and the mode shape variations amongst successive modes [29].

Devriendt used mode modal parameters information (frequencies, mode shapes and damping) to track their evolution under WT parked conditions for 14 days [31]. This methodology proved to be effective at identifying frequency and damping variations motivated by variant ambient and functioning conditions.

1.3. Objectives

The main objectives of this study rely on the automated modal tracking procedure, especially in the automated modal parameter selection to overcome some mode selection problems. To reach these, the presented goals were defined:

- Comprehending the principles and concepts behind operational modal analysis.
- Understanding the elements that compose wind turbines and their structural dynamics.
- Pre-processing and analysing the collected acceleration time series.
- Characterizing the case study and extract valuable data to describe its behaviour.
- Improving of an in-house Automated Modal Analysis (AMA) methodology based on a density-based clustering technique [13].
- Investigating automated modal tracking procedures to obtain reliable tracked results.
- Critically analysing the thesis outcome and suggesting possible research paths.

1.4. Thesis Outline

The thesis is structured in seven sections:

- Section 2: an introduction of the theoretical concepts necessary to the thesis development is provided. In the first part, the OMA (Operational Modal Analysis) process is reviewed and the main formulations are presented. Follows the DBSCAN clustering technique revision.
- Section 3: the wind turbine structural elements are reviewed, followed by concepts associated to the dynamic behaviour of wind turbines.
- Section 4: the wind turbine characterization and operating conditions are revealed, followed by the monitoring setup description. Lastly, some preliminary results are presented to better comprehend the case study.
- Section 5: explains the research methodology. Firstly, the AMPS (Automated Modal Parameter Selection) procedure is detailed, followed by the explanation of the methodology utilized to perform modal tracking.
- Section 6: the results of implementing the methodology are provided. In the first subchapter, the AMPS procedure impact is disclosed and, in the second, the automated modal tracking outcomes are revealed.
- Section 7: the work conclusions are shortened and potential improvements or possibilities for future research are highlighted.

2

THEORETICAL BACKGROUND

2.1. Operational Modal Analysis

Operational Modal Analysis (OMA) is a method that, based only in the measured structural response, allows the estimation of the system modal parameters relying on a stabilization diagram.

To apply OMA, it is assumed a random excitation force in the form of white noise, meaning the force has equal magnitude for all the frequencies in the bandwidth of analysis. This allows the dynamic characterization of the structure since the modal parameters can be extracted from the mathematical model. This output-based method utilized is Frequency Domain Decomposition (FDD) and reconstructs the signal in the frequency domain, after estimation of autocorrelation and cross-correlation functions (ACF and CCF).

The correlation functions are time-domain based and are often used to detect signal patterns over time, by comparing a signal to a delayed version with increasing time lags. This autocorrelation function returns a value between -1 and 1, being close to one when the signal is periodic, and close to zero if the excitation is random.

The cross-correlation function has the same principle as ACF, however compares the signal with a reference signal, extracting the common response periodicities at the two comparison points. At least one reference point should be defined.

Applying the Discrete Fourrier Transform to the correlation functions, the time-domain data is converted to frequency-domain, and the power spectral density functions (PSDs) are generated. The cross-power spectral densities (CPSD) result from dividing the CCF by the frequency resolution. The auto-power spectral densities (APSD) are obtained analogously, as shown in equations (1) and (2).

$$APSD = \frac{G_{xx}}{\Delta f} = \frac{S_x \cdot \overline{S_x}}{\Delta f} \tag{1}$$

$$CPSD = \frac{G_{xy}}{\Delta f} = \frac{S_x \cdot \overline{S_y}}{\Delta f} \tag{2}$$

S_x and $\overline{S_x}$ are, respectively, the signal and its delayed complex conjugate, while $\overline{S_y}$ is the complex conjugate of the reference signal.

The stabilization diagram is derived from a curve-fitting process between the CPSD and APSD with an increasing order modal model. For each modal model, the modal parameters are determined (eigenfrequencies, damping ratios and modal vectors). Then, the stable poles are selected, and the mode shapes and the participation factors can be derived with a least-squares method [17].

Figure 2 schemes the operational modal analysis process from the measured time accelerations to the final stabilization diagram, estimated with a curve-fitting method.

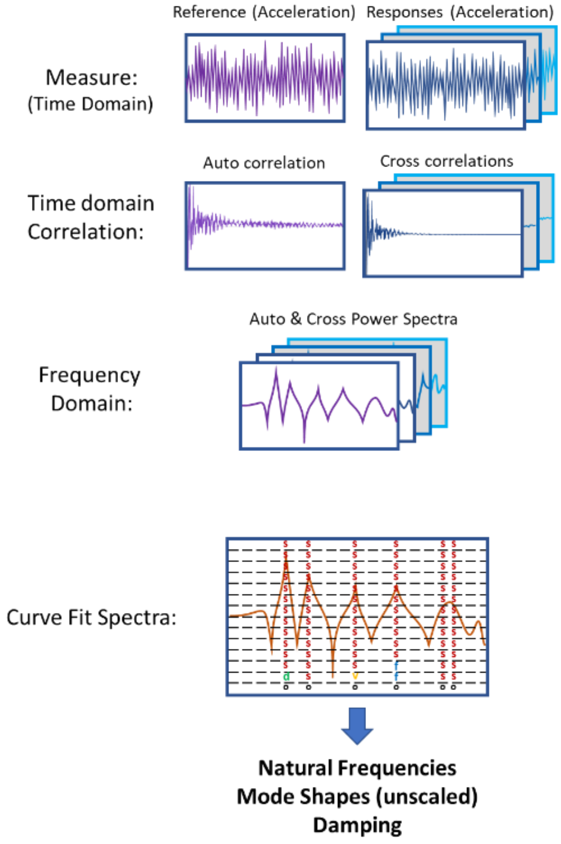

Figure 2 - Operational Modal Analysis Process [32].

2.1.1. MODAL MODEL

The modal model is a model to estimate the modal parameters relying on the output spectra, obtained from the measured time datasets. This model provides a good understanding of the physicality behind the problem from an engineering perspective [22].

For stationary stochastic processes, the auto and cross power spectral density matrix between the outputs (S_{yy}) of a system represented by the transfer function matrix $H(\omega)$ is given by equation (3):

$$\left[S_{yy}(\omega)\right] = [H(\omega)][S_{uu}][H(\omega)]^{H} \tag{3}$$

For a white noise type, the input is a constant power spectrum, and the auto and cross power spectral density matrix between the outputs (S_{yy}) can be directly derived from the measured responses. Afterwards, it is decomposed in modal components, as presented in equation (4):

$$\left[S_{yy}(\omega)\right] = \sum_{k=1}^{n_2} \frac{\varphi_k \cdot g_k}{i\omega - \lambda_k} + \frac{{\varphi_k}^* \cdot {g_k}^*}{i\omega - {\lambda_k}^*} + \frac{g_k \cdot \varphi_k}{-i\omega - \lambda_k} + \frac{{g_k}^* \cdot {\varphi_k}^*}{-i\omega - {\lambda_k}^*} \tag{4}$$

Where g_k are the operational reference factors.

For the full spectrum, given by equation (4), there are four poles per mode. For the half spectrum (equation (5)), the modal parameters can equally be derived, and there are only 2 poles for each mode.

$$\left[S_{yy}^{+}(\omega)\right] = \sum_{k=1}^{n_2} \frac{\varphi_k \cdot {g_k}^T}{i\omega - \lambda_k} + \frac{{\varphi_k}^* \cdot {g_k}^H}{i\omega - {\lambda_k}^*} \tag{5}$$

The sum of the dynamic system modes contributions defines the transfer function, equivalent to the frequency response function (FRF) by substituting s per $i\omega$:

$$[H(s)] = V \cdot (s \cdot I - \Lambda)^{-1} \cdot L^T = \sum_{k=1}^{n_2} \frac{\varphi_k \cdot {\gamma_k}^T}{s - \lambda_k} + \frac{{\varphi_k}^* \cdot {\gamma_k}^H}{s - {\lambda_k}^*} \tag{6}$$

With: V is the modal vector matrix

L is the modal participation factor matrix

Λ is the system poles diagonal matrix

Where n_2 is the number of modes, $\cdot^*$ is the complex conjugate of a matrix or vector, $\cdot^T$ is the transpose of a matrix or vector, $\cdot^H$ is the complex conjugate transpose (Hermitian) of a matrix or vector, φ_k is a column vector containing n_2 components of the mode shape k, γ_k is the system poles vector (modal participation factors) and λ_k are the system poles.

The operational reference factors are function of the modal parameters of the system and the constant input spectrum matrix, so its physical interpretation is not evident.

The poles exist in complex-conjugate pairs and are related to each frequency (f_k) and damping ratio (ξ_k) as presented in equation (7):

$$\lambda_k, {\lambda_k}^* = -\xi_k f_k \pm i\sqrt{1 - {\xi_k}^2} \cdot f_k \tag{7}$$

Where i is the imaginary unit.

2.1.2. Operational PolyMAX

PolyMAX, also designated poly-reference Least Squares Complex Frequency Domain (p-LSCFD), is the algorithm based on the weighted correlogram method for processing the power spectra between the outputs, defined as the Fourier transforms of the correlation vectors. Afterwards, a modal model is fitted to estimate the modal parameters.

The Discrete Fourier Transform (DFT) of the output correlation matrix is calculated by the weighted correlogram technique. If the DFT is extended to positive and negative time lags of the correlation function the spectrum is the result. The half-spectrum is obtained when the DFT considers only positive values, and this is sufficient to perform modal analysis.

In PolyMAX an exponential window is used before the DFT of the correlations to minimize Leakage problems. This window is compatible with the modal model and its effect on the damping ratios estimates can be corrected.

The p-LSCFD method works in the z-domain, a frequency-domain derived from a discrete-time signal, and the "right matrix-fraction model" is assumed to represent the measured half spectrum matrix (Equation (8)).

$$\left[S_{yy}^{+}(\omega)\right] = [B(\omega)][A(\omega)]^{-1} \tag{8}$$

The half spectrum matrix $\left[S_{yy}^{+}(\omega)\right]$ has a number of lines equal to the number of measured responses and the number of references defines the number of columns. $A(\omega)$ and $B(\omega)$ are polynomial matrices and are explicated in equations and (9) and (10), respectively. Equation (11) defines the polynomial basis function necessary to assess the polynomial matrices.

$$[A(\omega)] = \sum_{r=0}^{p} \Omega_r(\omega)[\alpha_r] \tag{9}$$

$$[B(\omega)] = \sum_{r=0}^{p} \Omega_r(\omega)[\beta_r] \tag{10}$$

$$\Omega_r = e^{i\omega\Delta tr} \tag{11}$$

Where p is the modal order, $[\alpha_r]$ the denominator matrix polynomial coefficients and the nominator matrix polynomial coefficients are $[\beta_r]$. Δt is the sampling period and the polynomial basis functions Ω_r are a frequency domain model derived from a discrete time domain model (z-domain model). [33]

After the equations' linearization, the PolyMAX estimates the matrices polynomial coefficients as the least-square solution between the measured output and the theoretical one obtained through equation (8). Then, the stabilization diagram is designed for increasing modal order (p), using the reduced normal equations.

Figure 3 is a stabilization diagram, where the horizontal axis computes the damped frequency range and the vertical axis the modal model order. For each model order, the poles identified through the modal model are computed until is reached the maximum model order, for which the function describing the modal model is graphically represented.

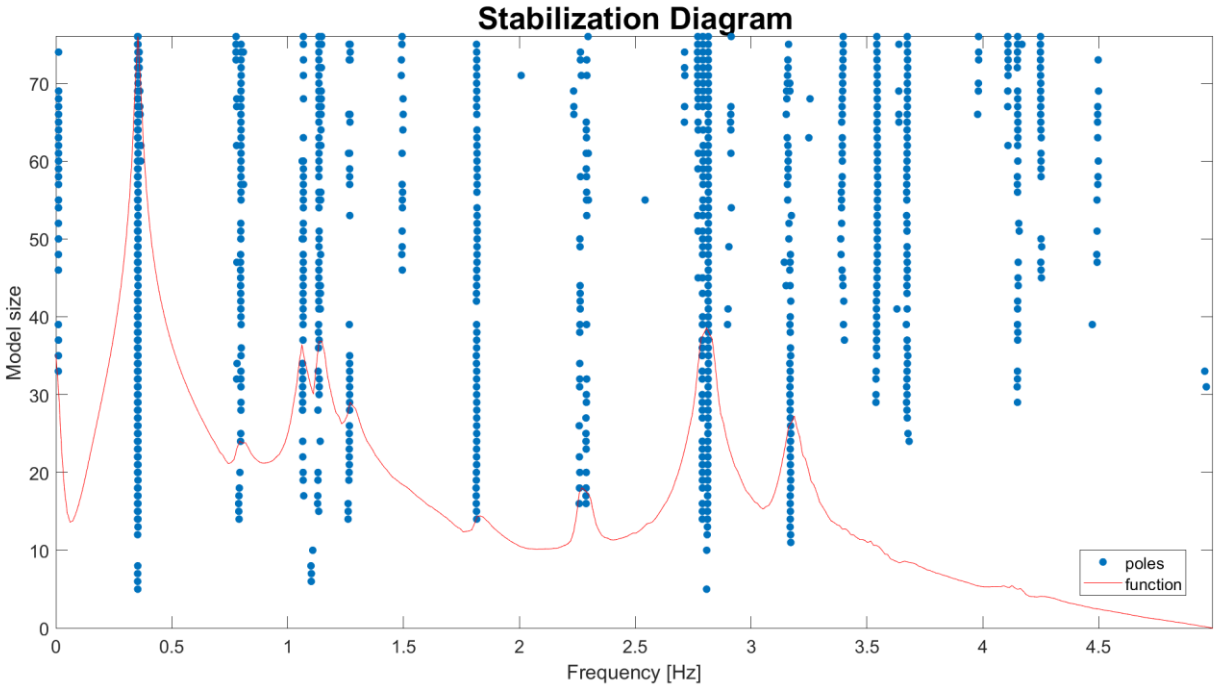

Figure 3 - Stabilization Diagram, from MATLAB.

The natural frequencies, the damping ratios and the operational reference vectors are calculated. One of the primary benefits of this method is its applicability to closely spaced poles, as the clarity of stabilization diagrams enhances the selection of system poles compared to other methods. The model order over-selection leads to an enhanced parameters estimation accuracy.

Lastly, the mode shapes are derived from the pole-residual model, explicated by equation (12):

$$[S_{yy}^{+}(\omega)] = \sum_{k=1}^{n_2} \frac{\varphi_k \cdot g_k}{i\omega - \lambda_k} + \frac{{\varphi_k}^* \cdot {g_k}^*}{i\omega - {\lambda_k}^*} - \frac{LR}{i\omega} + i\omega UR \tag{12}$$

Where n_2 is the number of modes, $\cdot^*$ is the complex conjugate of a matrix or vector, φ_k is a column vector containing n_2 components of the mode shape k, g_k are the operational reference factors, λ_k the system poles and LR and UR are, respectively, the lower and upper residues.

2.1.3. Modal Assurance Criterion

The Modal Assurance Criterion (MAC) is one of the most used methods to quantify the similarity of mode shapes and can be applied to any vectors [34].

MAC relates the degree of linearity between two modes, corresponding to the normalized scalar product of two vectors ϕ_A and ϕ_B, and further presented in equation (13):

$$MAC(r,q) = \frac{\left|\{\phi_A\}_r^T\{\phi_B\}_q^*\right|^2}{(\{\phi_A\}_r^T\{\phi_B\}_r)\left(\{\phi_A\}_q^T\{\phi_B\}_q\right)} \tag{13}$$

In a more general way, it can be applied to complex vibration modes ($\psi_A$and ψ_B), resulting in equation (14):

$$MAC(r,q) = \frac{\left|\{\psi_A\}_r^T\{\psi_B\}_q^*\right|^2}{(\{\psi_A\}_r^T\{\psi_A\}_r^*)\left(\{\psi_B\}_q^T\{\psi_B\}_q^*\right)} \tag{14}$$

This correlation factor assumes values between zero, when the vectors are linearly independent, and one, when the two shapes are proportional. This least squares-based linear regression analysis is more sensitive to large differences between comparative values, while small magnitude variations are imperceptible in the MAC [35].

The MAC values are often presented as a 2D matrix plot illustrating the correspondence between modes, being the axis x and y the modes indexes. Figure 4 shows a measurement MAC matrix, where each square corresponds to the MAC scalar between two modes. The diagonal red tiles indicate the modes shapes are proportional to itself and the blue tiles, associated to MAC inferior to 0.2, reflect almost orthogonal mode shapes. The tiles with other shades are associated mode shapes with some correlation [36].

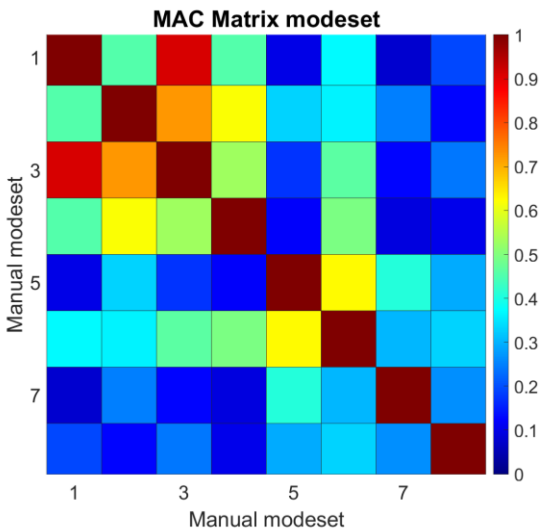

Figure 4 - MAC matrix for a time series.

2.2. DBSCAN: Density-Based Spatial Clustering of Applications with Noise

DBSCAN is a clustering density-based technique, where clusters are defined based on a measured distance. The necessary inputs are the radius (ε) and the minimum number of points ($minpts$) that should fit inside a neighbourhood of a point to define a cluster. When compared to other clustering techniques, this is faster, simpler and doesn't require a predefinition of the final clusters number, being very adaptable to different cluster shapes.

This clustering technique divides the poles in three categories: core, border and noise points. The core point has inside its radius at least the minimum number of points, which are all immediately associated to that cluster, though they can be classified as core themselves (if the conditions are verified, contributing to the cluster's propagation), or as a border point if inside that pole radius the minimum number of poles is not reached. The noise points don't verify the criteria and are not assigned to clusters. After analysing all the points, they must be either assigned to a certain cluster or classified as noise as illustrated in Figure 5 [13]. This machine learning procedure was implemented in the methodology used in this work, as explained in Section 5.1.

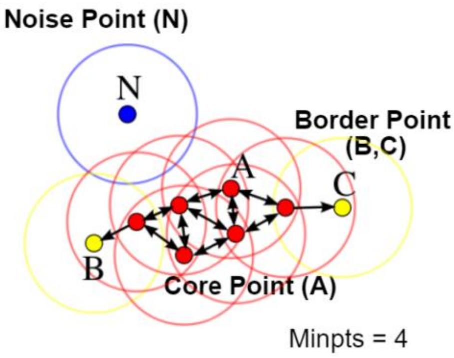

Figure 5 - Illustration of DBSCAN's principles [37].

3

WIND TURBINE FUNCTIONING & DYNAMIC

The available wind turbines can be divided into two main categories, accordingly to the position of the rotor axis of rotation: vertical-axis and horizontal-axis wind turbines. The last ones are the most common solution and can be divided in two classes: upwind and downwind rotors, being this last solution obsolete nowadays due to associated noise, vibrations and efficiency problems.

The case study further presented in Section 4 involves a horizontal-axis upwind onshore wind turbine, so this chapter is intended to present their structure, components and functioning with a theoretical approach.

3.1. STRUCTURAL ELEMENTS

A horizontal-axis upwind onshore wind turbine is divided in four main elements: the rotor, moving component according to the wind velocity; the nacelle, where the power is generated and the control systems are installed; the tower that supports the upper components and whose slenderness can lead to dynamic problems; and the foundation, ensuring structure's stability and driving the loads to the soil.

Figure 6 depicts these main elements and locates some other components, while the degrees-of-freedom commonly used to describe the dynamics of wind turbines are illustrated in Figure 7. A detailed description of the rotor, the nacelle and the foundation are presented in the next subchapters.

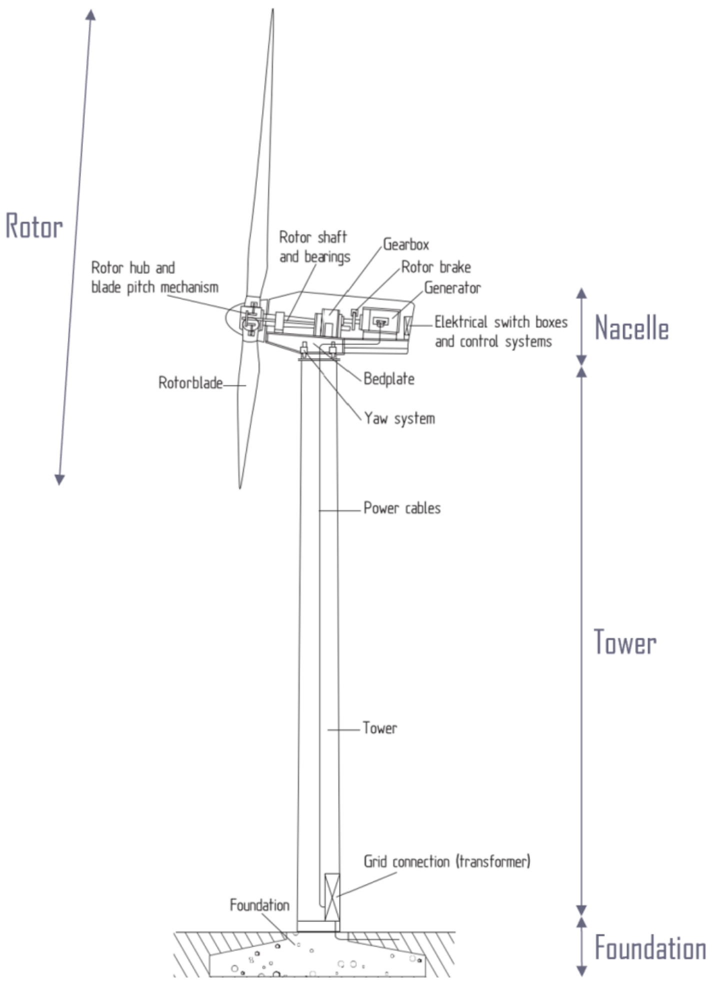

Figure 6 - Main Components of a Horizontal-axis Upwind Onshore Wind Turbine (adapted from [38]).

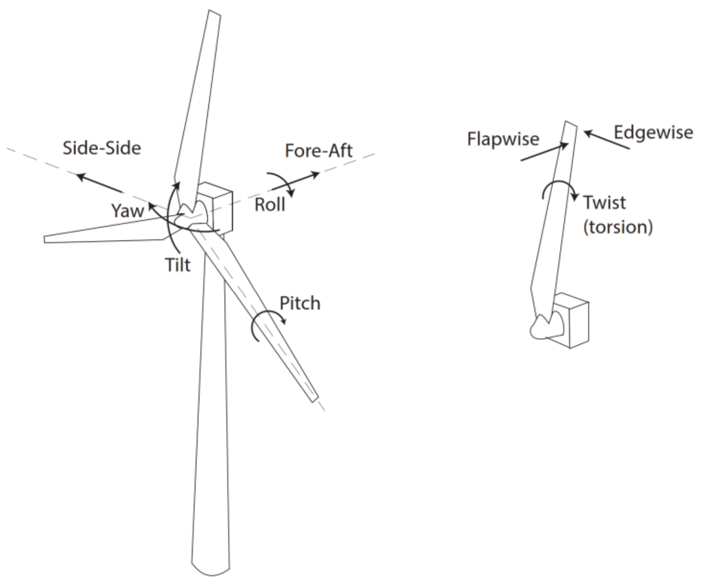

Figure 7 - Terminology of the Wind Turbine main Axes of Translation and Rotation [20].

3.1.1. Rotor

The system blades plus hub connection compose the rotor, presented in Figure 8, responsible for the wind kinetic energy to rotor kinetic (rotational) energy conversion.

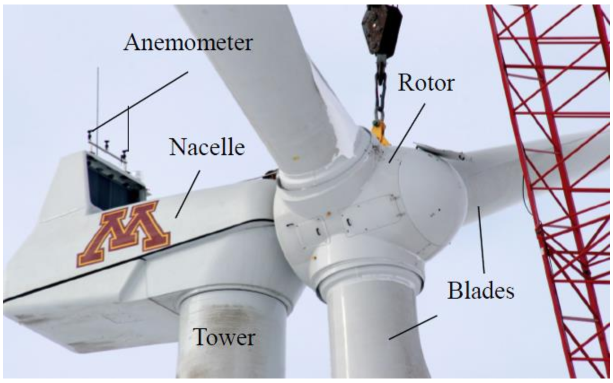

Figure 8 - Wind Turbine Rotor [39].

The blades design is an important field, allowing the wind energy extraction optimization. Therefore, their airfoils (cross-section shapes) are complex and vary along their length. In addition, a compromise between weight, stiffness and strength must be fulfilled to avoid high gravitational loads (for both the tower and the blade itself), not to deflect too much since it directs to efficiency losses and could lead to tower-blade collision and, lastly, to resist an enormous number of cycles during its lifetime. Composite materials are a prominent solution allowing light, stiff and strong blades and the most common solutions are epoxy resins combined with glass fiber or carbon fiber.

The rotor configuration also depends on the blades number, which is associated to different vibration problems, tip-speed and efficiency. Historically, wind turbines have between one and three blades. Analysing the Figure 9, where the yaw moment created by an asymmetrical wind flow on wind turbines with varying number of blades is presented, it is concluded that this moment is minimized for a three or more blades solution. This occurs because the less blades exist the higher the moment of inertia asymmetry, leading to a high variation load profile during the rotor revolution. For solutions with at least three blades this effect is almost imperceptible, such as the time-varying yaw-moment associated to the described phenomenon.

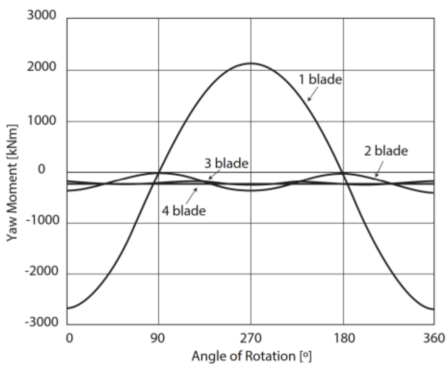

Figure 9 - Yaw moment, on wind turbines with different number of blades, caused by asymmetrical wind flow (adapted from [38]).

To diminish the effects of this additional loads on the wind turbine, solutions focused on increasing the tower-hub connection flexibility were developed, such as the teetering hub or the flapping hinge rotor.

The first option presented is applicable to two blades rotor and balance some asymmetrical loads by allowing the rotor to teeter about the rotor shaft due to a hinge in the hub. The last flexible solution is made of a hinge located at each blade allowing individual blades regulation.

The rigid hub connection is the simplest solution and most common among two and three blades rotors. In this case, the blades have a fixed position related to the hub and there is a direct load transfer from the hub to the drive train.

3.1.2. Nacelle

The nacelle is composed by electrical and mechanical elements associated to the power production and to the rotor motion.

The rotor kinetic energy is received by the rotor shaft, which is connected to the gearbox. The gear box transforms the rotor speed in a higher value more suitable for the generator, responsible for transforming the mechanical energy in electrical energy. This unfolding rotation is operated by the generator drive shaft.

This main component also holds a mechanical breaker to stop the turbine when needed and a yaw system to orient the nacelle according to the wind direction. A bedplate supports all these components. Figure 10 shows an internal cross-sectional view of the nacelle.

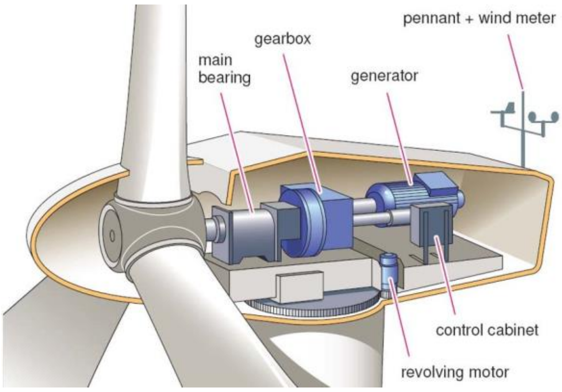

Figure 10 - Nacelle Internal View [40].

3.1.3. Foundation

Onshore wind turbines adopt generally traditional civil engineering foundation solutions, namely slab foundations or pile foundations represented in Figure 11.

Reinforced concrete slabs with polygonal shapes are the most common solution when the soil has a good bearing capacity. The adopted shape provides resistance to the overturning moment given by the eccentricity of the reaction. The total load is dispersed by the foundation area and the friction soil-foundation, specifically the vertical and horizontal components of the total acting load.

Pile foundations is a solution adopted for low bearing capacity soils and drive the acting loads for deeper soil layers with higher resistance through axial and lateral pile resistance. This solution is composed by a pile cap connecting a certain number of piles, extended until there is a total load transference to the soil layers.

a)

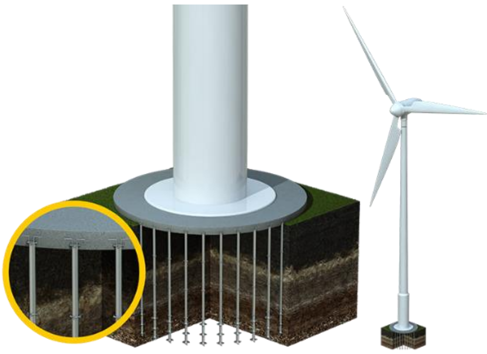

b)

Figure 11 - Onshore wind turbines foundation types: a) Reinforced concrete slabs [41]; b) Pile foundation [42].

3.2. Structural Behaviour of Wind Turbines

As previously presented, the wind turbines are highly dynamic structures, whose operation is conditioned by the dynamic excitations. Those are, in the case of onshore wind turbines, the environmental conditions, namely the wind speed, turbulence, and wake effect, and the operating conditions, specifically the rotor rotating and the associated inertia effect of the blades' rotation (further explained).

To avoid resonance problems while in operation and to better comprehend the structural behaviour of the wind turbine, a multi degree-of-freedom model can be made, considering the mass, damping and stiffness properties [43].

3.2.1. Damping

To characterize dynamically the wind turbine, damping is a main parameter to be obtained. For onshore wind turbines, the main components contributing to the final damping are the structural, aerodynamical and the soil damping. However, in some cases, dampers can be installed at the tower to attenuate the vibration for a specific mode imposing a damping enhancement.

Structural damping is associated to the energy absorption by internal friction and energy conversion to heat, being an intrinsic value to the structure. Different tower concepts, materials, and connections of the tower components and to the soil (foundations) interfere in the final structural damping value.

The interaction between wind flow and structure motion is responsible for the aerodynamic damping, a considerable part of the total damping. This is favourable when the turbine is oriented in the wind direction and should be considered in the design stage and to perform life cycle assessment.

This damping contribution depends on the relative velocity between structure and flow, so its magnitude increases as the wind speed and the drag force are rising. If, for the same operational conditions under different wind speeds, it is performed a comparison between the damping values, the aerodynamic damping contribution can be assessed [31].

Under operation conditions, the aerodynamic forces act mainly in the rotor out-of-plane direction, so the first for-aft (FA) vibration mode is the one where the aerodynamic damping has the higher influence on the total value. Thus, in the side-side (SS) direction, the opposite one, since the aerodynamic forces are almost negligible, the aerodynamic contribution to damping is practically null. Note that if the pitch is enhanced, the dynamic behaviour observed might be the opposite.

Material damping and geometrical dissipation (radiation damping) are the factors contributing to soil damping. The first one is associated to the internal friction among the soil grains and the second component is linked to the energy wave propagation in the soil.

Near a shallow foundation, both factors contribute to energy dissipation, however as the distance from the foundation increases the material damping loses importance and the geometrical attenuation becomes the only one acting [44].

To note that soil damping is a parameter with high variability due to high heterogeneity of soil conditions, and very difficult to estimate. Nevertheless, the total damping might have a relevant contribution of this parameter [45].

3.2.2. Cyclic Vibration Loads

As previously mentioned, a wide number of dynamic loads stress the structure. Here, the cyclic ones are object of analysis due to their relevance to the structure response. When the structure is subject to cyclic loads, some of the recorded peaks correspond to this acting dynamic load and not to frequencies associated to the structural behaviour. Therefore, the frequencies associated to cyclic load should be previously identified and can be associated to multiple origins: aerodynamic force and mass unbalance.

Since the wind turbine in analysis is three-bladed, the cyclic loads acting is almost exclusively due to aerodynamic forces, namely:

- Rotational Sampled Turbulence Spectrum: each blade passing through the tower leads to an excitation of $N_B\,\Omega$, being this the aerodynamic rotor excitation (N_B is the number of blades), and 1Ω is associated to each blade transition over the gust.

- Tower Shadow Effect: the perturbation imposed to the wind flow by the tower leads to a decrease in the wind speed in that area and, consequently, to a decrease of the force acting on the blade when it is positioned right in front of the tower. This phenomenon causes a cyclic excitation in the blades and in the tower. This effect is higher for down-wind rotors once the wind flow is perturbed by the tower, retarding the flow excitation in the blades.

- Vertical Wind Shear: the wind speed increases in height and, for increasing rotor diameters, a notable wind speed variation is noticed between the top and bottom rotor positions. Therefore, every revolution, each blade experiences the extreme values of wind load.

An Average Normalized Power Spectral Density (ANPSD) function is illustrated in Figure 12, for an acceleration measurement with rotor constant speed of 12.3 rpm. The red dashed lines observed state for the rotor speed harmonic frequencies ($1\,\Omega$, $3\,\Omega$, $6\,\Omega$, $9\,\Omega$, …) position due to blades passage aligned with the tower.

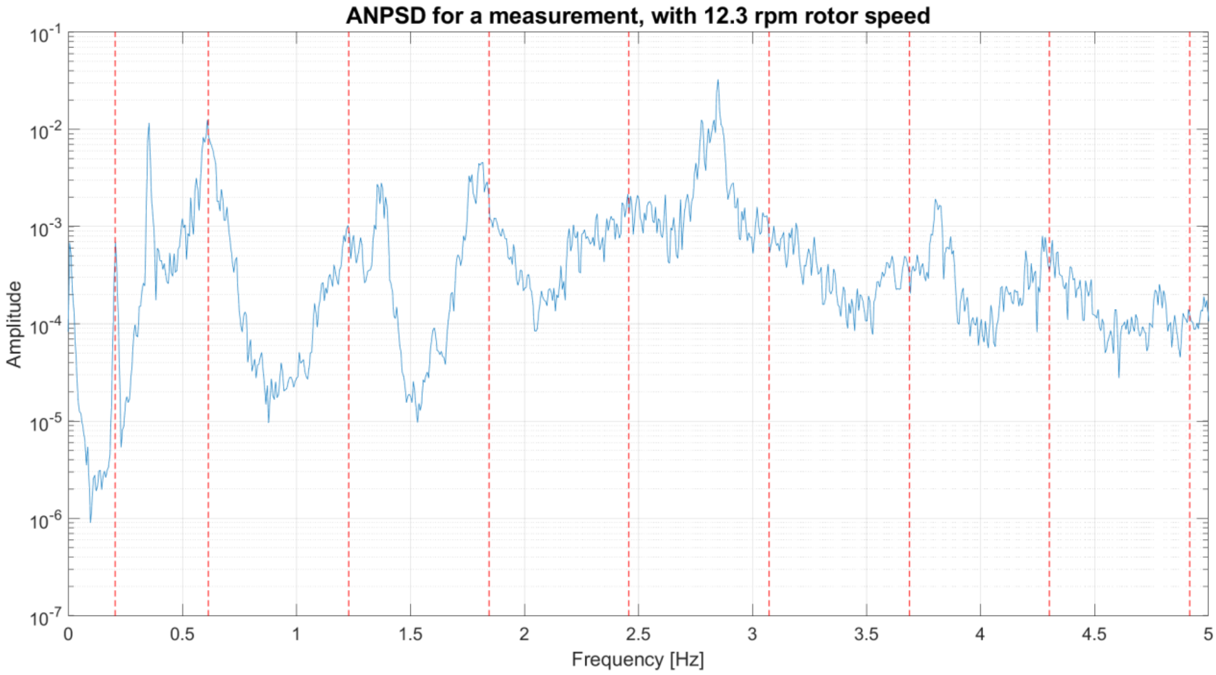

Figure 12 – Representation of an ANPSD function with vertical dashed lines showing the position of the harmonics due to blades rotation.

Regarding the design phase, the structural natural frequencies should be distant enough from the rotor frequencies and associated blades rotation harmonics. Otherwise, there's a resonant response that may cause fatigue problems, damage or even failure [46].

For increasing rotor diameters, the tower shadow effect and the vertical wind shear rise accordingly. Figure 13 presents a schematic wind profile diagram and it can be concluded that the higher the hub is located the feeble is the vertical wind shear, however the tower shadow effect is not correlated to this parameter [47].

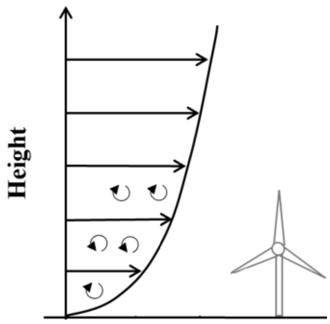

Figure 13 - Schematic diagram of Wind Profile (adapted from [48]).

An unbalanced rotor, due to ice accumulation in the blades or manufacturing defects, imposes a rotating force that excites lateral vibrations in the rotor nacelle and tower and overloads the 1 Ω frequency.

3.2.3. Dynamic Characterization of the Tower

The wind turbine structural system can be simplified as a simple cantilever beam, with mass distributed along height and a mass concentrated at the nacelle, including the rotor. This initial assumption can be used to access the frequency associated to the first mode [49].

The rotor is a component positioned in a determined direction; therefore, the wind turbine tower is slightly asymmetrical and its analysis should be accessed in two planes: side-side (SS) and fore-aft (FA). Figure 14 presents these directions and the first order mode shapes.

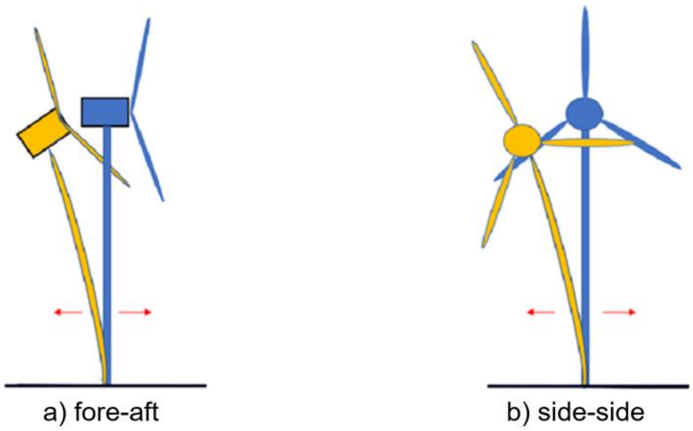

Figure 14 - Vibration modes for fore-aft (a) and side-side (b) directions: undeformed (blue) and deformed (yellow) (adapted from [50]).

Figure 15 shows the first, second and third theoretical mode shapes. As the mode order increases, the complexity of the curve also raises. The first order mode shape is a curve descripting a lateral movement progressively increasing from the basis to the top of the tower. The second mode shape has one node. For increasing order mode shapes the number of nodes increases proportionally, accompanying the mode shapes complexity.

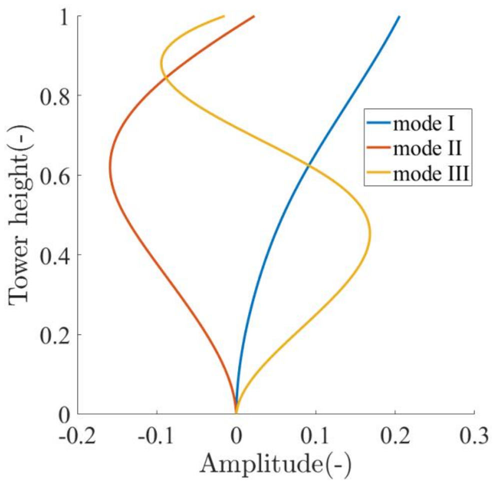

Figure 15 - Expected mode shapes for the three first vibration modes [51].

The reduced asymmetries experienced by wind turbines' structure and soil conditions lead to closely spaced FA and SS modes, for modes of all orders. Due to varying environmental and operational conditions, their frequencies may even cross each other, during the tracking process [31].

The mode shapes dominated by the rotor also produce tower deflections, represented in this work by *. Figure 16 presents an example of the expected mode shapes for the vibration modes until the 3rd order, plus the 4FA mode.

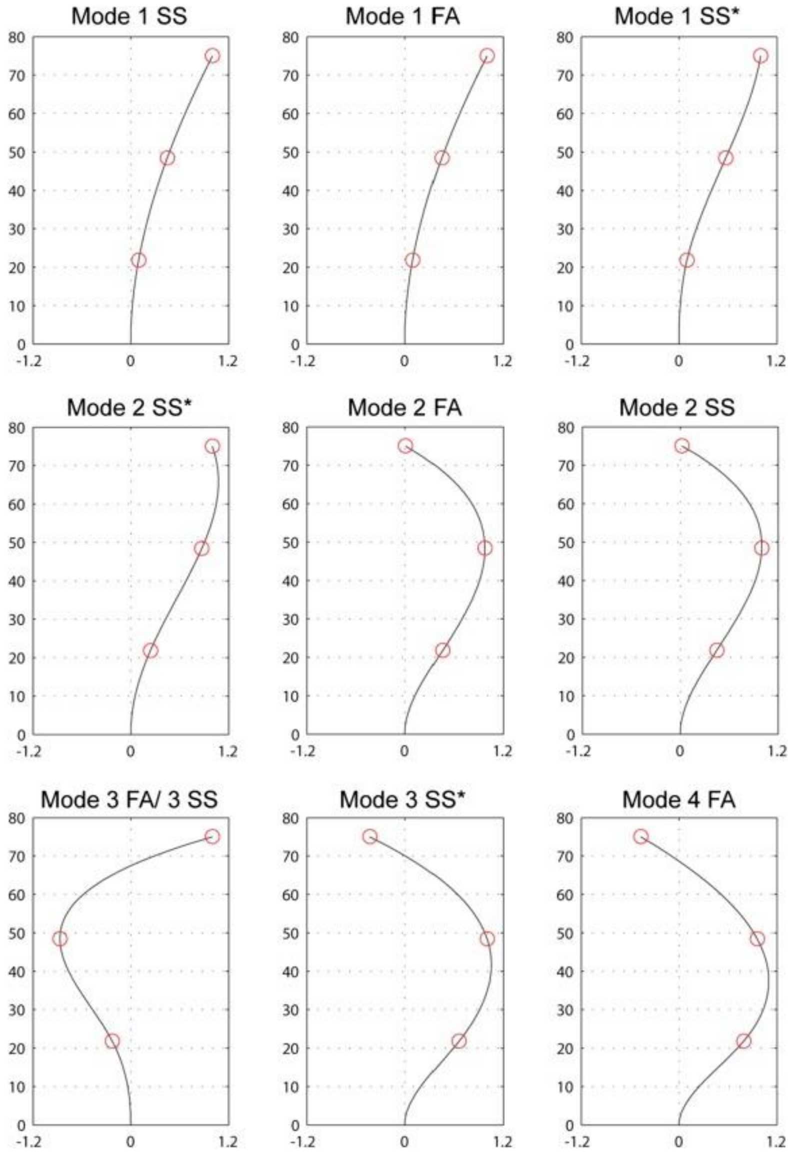

Figure 16 - Expected tower mode shapes, based on [29].

4

CASE STUDY

4.1. DESCRIPTION OF THE WIND TURBINE

The present case study is a 2.0MW onshore wind turbine located in Portugal (Figure 17).

Figure 17 - Wind Turbine under research focus.

This specific model monitored has three pitch-controlled blades and an up-wind rotor whose operation conditions vary accordingly to the wind.

The wind turbine is founded in a reinforced concrete slab foundation. The steel tubular tower is composed by three segments, assembled by bolted flanged connections. The hub is located at 80 meters and the rotor has 82 meters of diameter.

4.2. Operating Conditions

For a wind speed varying between 3 and 25 m/s, the wind turbine is operating, and for wind speeds higher than 13 m/s the rated power is reached, as expressed in Figure 18. The six different regions defined explicitly in the figure are related to the wind turbine operating conditions.

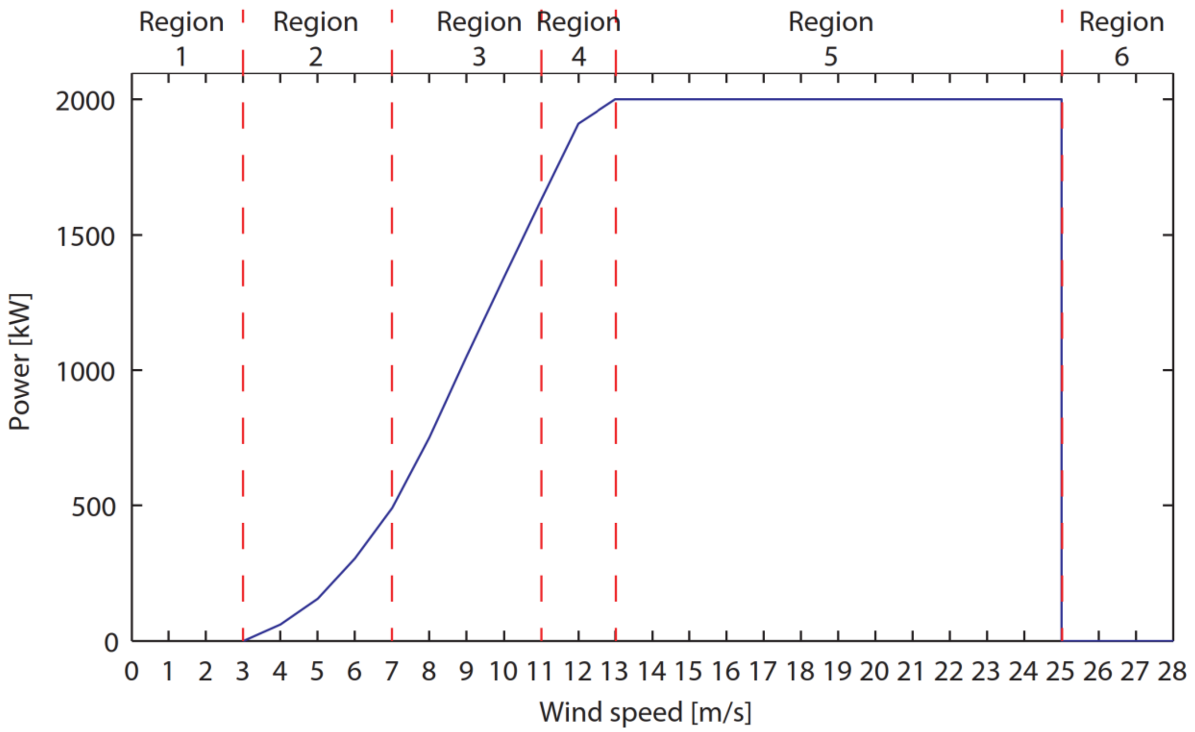

Figure 18 - Wind Turbine Theoretical Power Curve [20].

The first region is characterized by diminished wind speeds, for whom the machine is parked or idling, and the upper-limit corresponds to the cut-in speed of the wind turbine. In this phase, there is a constant analysis of the wind conditions to define the feasibility of starting operating.

Entering region two, and if the rotor torque is consistent for a wind speed above the cut-in value, the wind turbine starts the power production regime, where the tip-speed ratio is close to optimal and the rotor speed varies notably. In the next region, while the wind speed increases, the rotor torque achieves its rated value. In both phases, the yaw actuator orients the rotor in the wind main direction and the blades pitch angle assume the minimum value, allowing the maximum lift force on the blades and optimizing the power production [52].

Increasing the wind speed and after the rotor rated speed is achieved, the blades pitch angle decreases to maintain the rotor torque within defined operation limits, which consists of the fourth region. When the power limit is reached comes region five, the last power production region. In this one, the power production is kept constant by increasing the blades pitch while wind speed increases, to keep the rotor torque at its maximum allowed value. These limits are defined to avoid electrical and mechanical overloads, which could risk the operational and structural integrity of the wind turbine.

For wind speed above 25 m/s, the production is stopped because the acting loads are excessive, and the blades pitch assume 90°.

Figure 19 enhances the real relation between the power generated and the wind speed registered. The real behaviour captured is similar to the theoretical curve anteriorly presented (Figure 18).

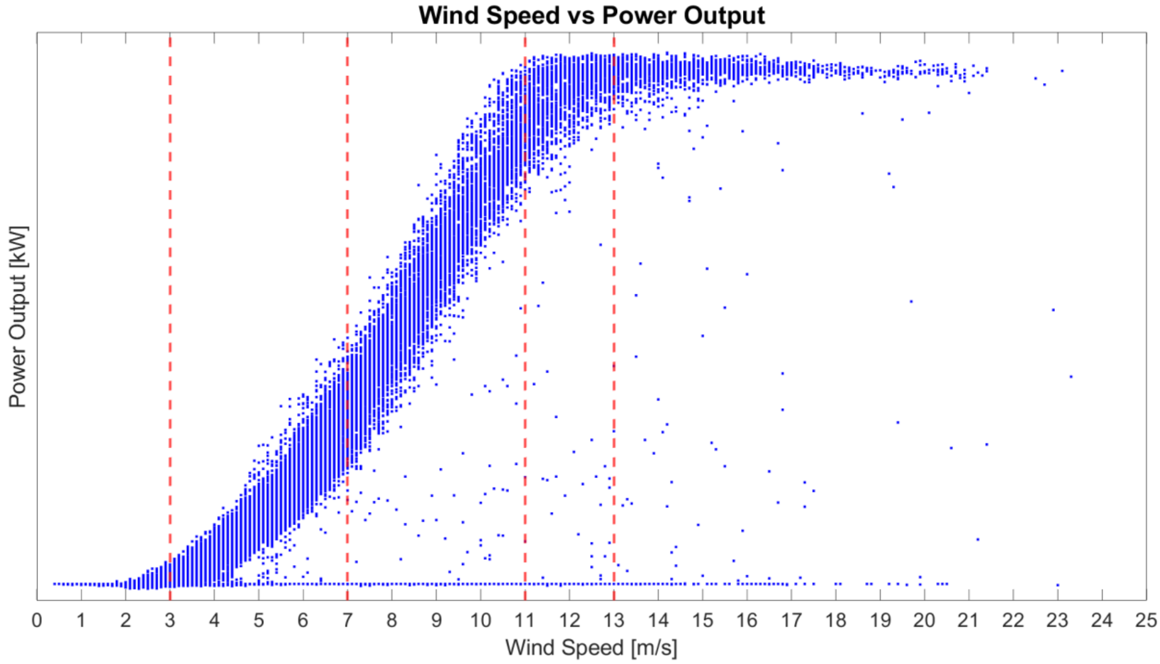

Figure 19 - Wind turbine power curve based on real measured data over one year.

Figure 20 explicit the evolution of the rotor speed with the wind speed for the monitored period, where is visible the wind turbine asynchrony functioning. The points dispersion registered for rotor speeds bellow 8.8 rpm and for wind speeds between 2 and 4 m/s are associated to data sets collected in transition phases from parked to operating conditions.

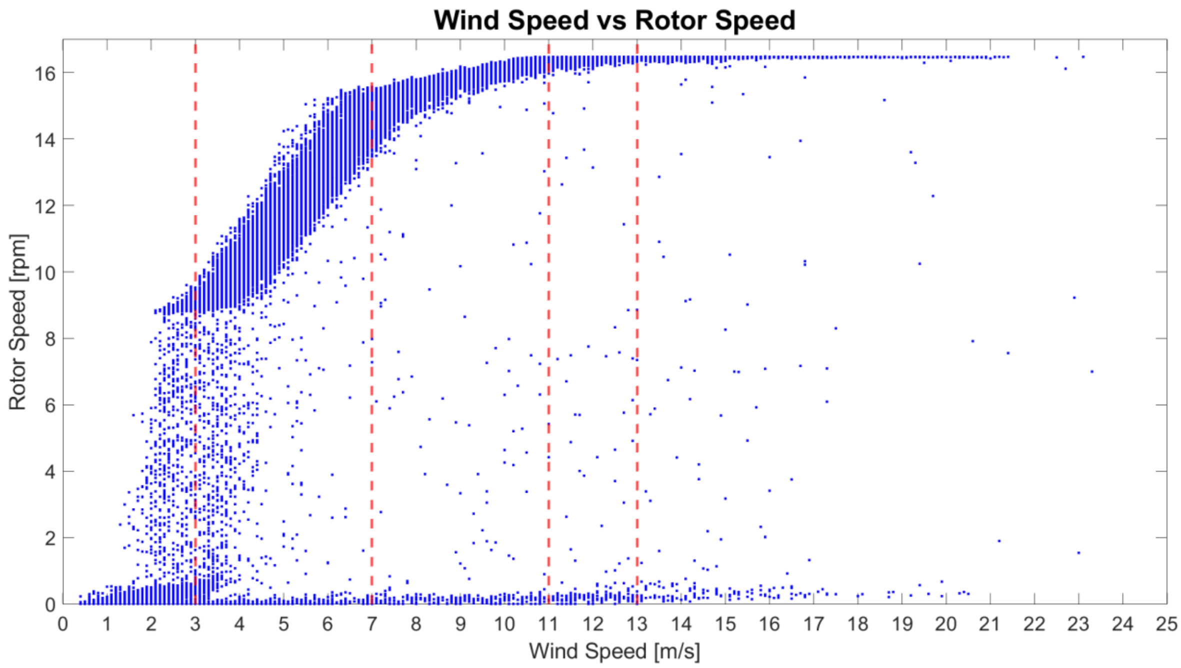

Figure 20 - Rotor speed evolution with wind velocity.

The progression of the blades pitch angle with the rotor speed is presented in Figure 21, exhibiting the wind turbine operational conditions previously presented. Bellow the rated wind speed, around 11 m/s, the blades pitch presents a pitch angle able to optimize the power production. When this value is reached, the turbine enters in protection mode, reducing the pitch angle to reduce and control the aerodynamic loads that it is subjected to [54]. This corresponds to the fourth operating region and to rotor speeds between 8.8 rpm and the value when the power output limit is reached. Therefore, the pitch angle increases progressively to protect the blades from damaging loading [52].

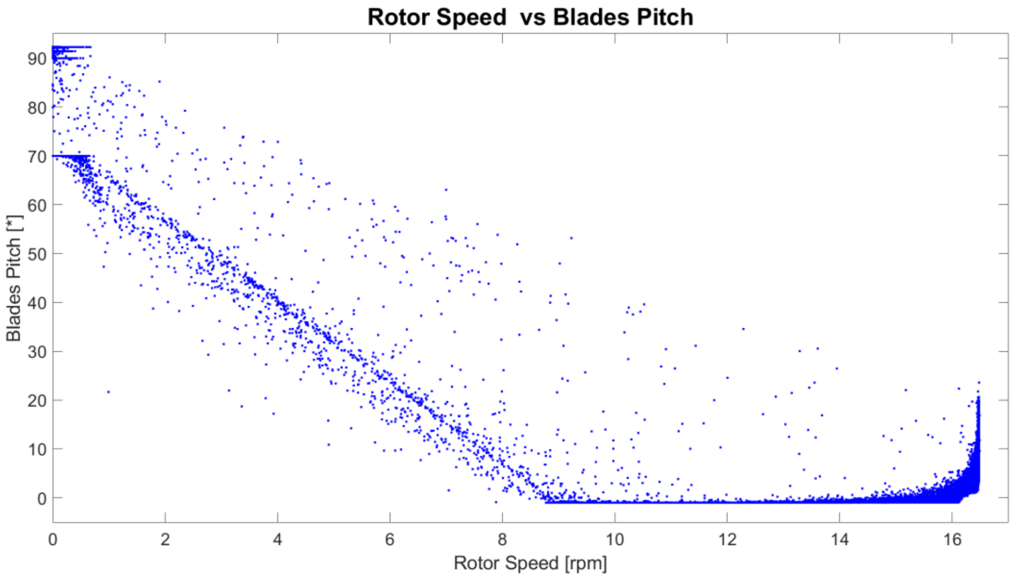

Figure 21 – Blades pitch evolution with rotor speed.

Figure 22 introduces the graph showing the pitch angle variation with the wind speed. Until the cut-in wind velocity is reached the blades are rotating slowly and the pitch range varies between 70° and 90°. When the production starts the pitch angle decreases to 0°, where it is kept until the rotor rated speed of 8.8 rpm is reached, in the fourth region. For wind speed greater than the rated value of 11 m/s, not to compromise the wind turbine integrity, the blades pitch increase [19].

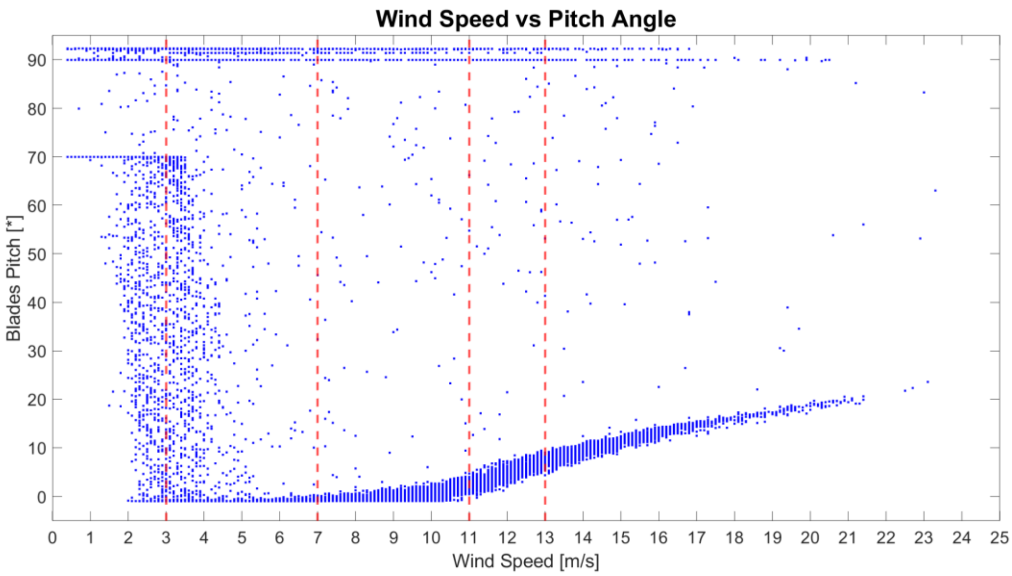

Figure 22 - Variation of blades pitch with wind speed.

The evolution of power production with increasing rotor speed is explicit in Figure 23. Three main regions that can be identified: the first region while the wind turbine is idling, and the power generated is null; the second region corresponds to the fourth operating area and the last region occurs for wind speed above the rated level, where an abrupt grow of power generated is recorded for a minimal rotor speed variation.

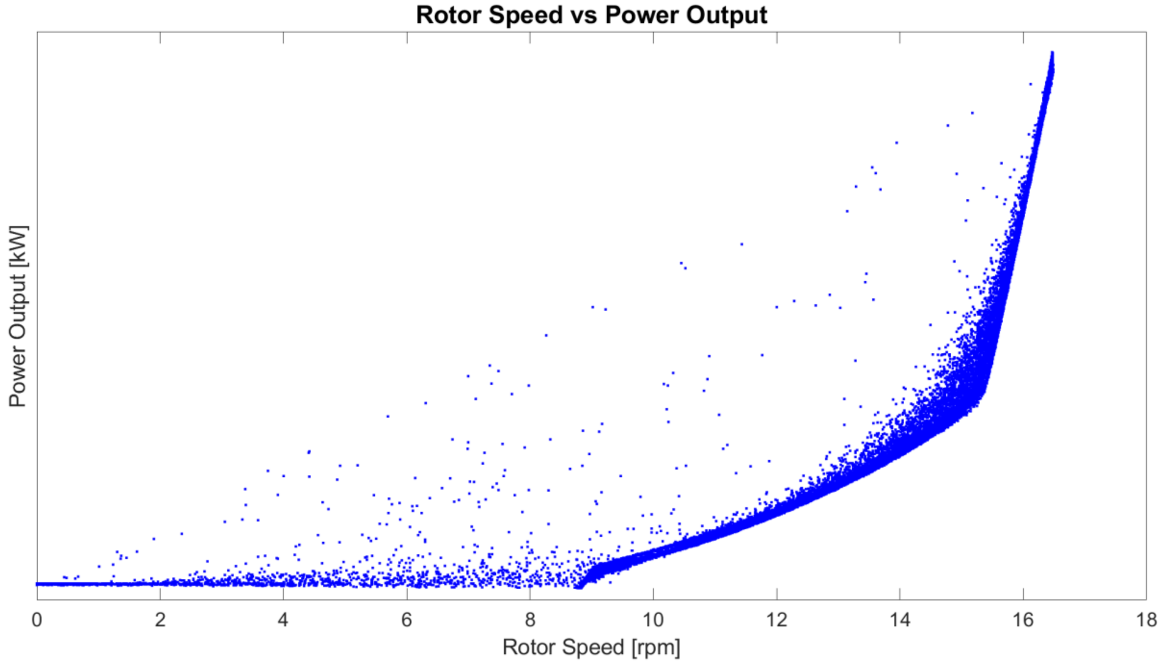

Figure 23 - Relation rotor speed with power output.

4.3. MONITORING SYSTEM

The wind turbine is equipped with six uni-axial accelerometers distributed along the tower height, as represented in Figure 24. The chosen layout allows the measurement of accelerations in two perpendicular directions at the three sections instrumented.

All the sensors are connected to a central acquisition system located at the internal first platform, at +20.000 meters. The force balance accelerometers are installed inside the tower, whose connection to the tower flanges is done with fixing clamps.

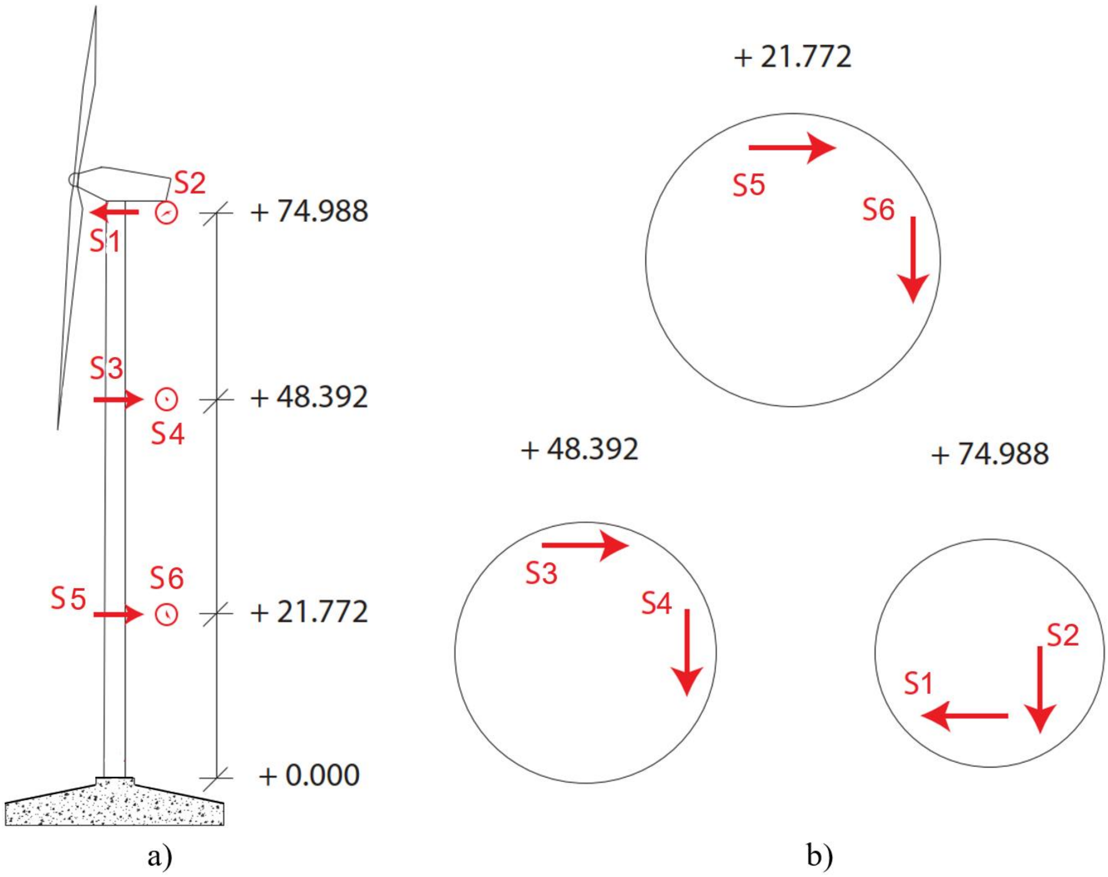

Figure 24 - Position of the accelerometers in three levels of the wind turbine: a) front view; b) cross-sectional views.

The accelerometers are force-balance sensors (Figure 25 a)), with a range of 140 dB, a frequency band from DC to 100 Hz and a measuring range varying from ± 0.1g to 4.0g. The acquisition system, presented in Figure 25 b), is constituted by a computer , to control the recording operations and store the recorded data, and a digitizer . The last component can connect to nine uni-axial accelerometers and, has a 24-bit analog-to-digital converter.

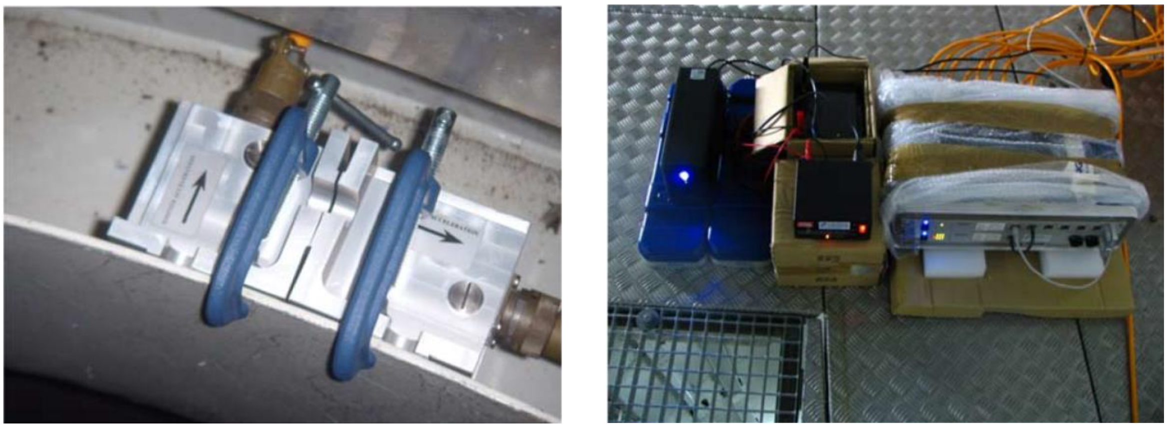

a) b)

Figure 25 – Monitoring system: a) accelerometer installed at the top tower flange; b) Central acquisition system.

This acquisition system was configured to record with a sampling frequency of 50 Hz and in a 10-minute acceleration time series. This last parameter was chosen to pair the SCADA system sampling period, once the two datasets complement mutually.

The SCADA system records mean, maximum and minimum values of a variety of environmental and operational parameters, such as:

- Wind Speed and Direction,
- Rotor Speed,
- Yaw Angle,
- Blades Pitch Angle,
- Power Output,
- Nacelle Position,
- Outdoor Temperature.

On the 22nd of July of 2013 the wind turbine monitoring process started, however the operation was not continuous in time due to problems in the electrical power supply of the acquisition system. This event could not be corrected immediately since access to the equipment was limited to maintenance periods.

A total of 37 685 data sets were recorded between 22/07/2013 and 21/07/2014. In the scope of this work only acceleration setups correspondent with SCADA data recorded were used once the analysis is performed based also in the rotor speed.

4.4. Preliminary Results

A colour map graph generated with the Averaged Normalized Power Spectral Density (ANPSD) functions of each 10-minute acceleration time series, ordered by rotor speed, is presented in Figure 26. The two red alignments around 0.35 and 2.8 Hz represent higher energy in the spectra and are associated to structural vibration modes. Other varying alignments with rotor speed are identified in the graph and are linked with the harmonic excitation due to blades rotation or rotor modes.

When analysing only one direction individually, Figure 27 and Figure 28, it is more perceptible the frequency alignments associated to side-side and fore-aft modes described in subsection 3.2.3. The 0.35 and 2.8 Hz lines are associated to the first and second order modes, appearing both in the SS and FA direction. The third alignment is more subtle, near 3.7 Hz, being more evident in the SS direction due to its superposition with the 3SS* mode once this alignment is not completely rectilinear. The 4FA mode is identified around 4.3 Hz.

The modes 1SS* and 2SS*, exist due to the whirling phenomenon occurring for rotating machines. The rotor rotation excites the tower at two frequencies (approximately 1.3 and 1.8 Hz) and, as the rotor speed increases the 1SS* frequency decreases and the other mode frequency registers the opposite tendency.

The rotor speed harmonic frequencies (1 Ω, 3 Ω, 6 Ω, 9 Ω) can also be identified with proportional variation and appearing at the following frequencies for the rated rotor speed: 0.27, 0.8, 2.5, 3.4 Hz. These are more evident in the combined colour map.

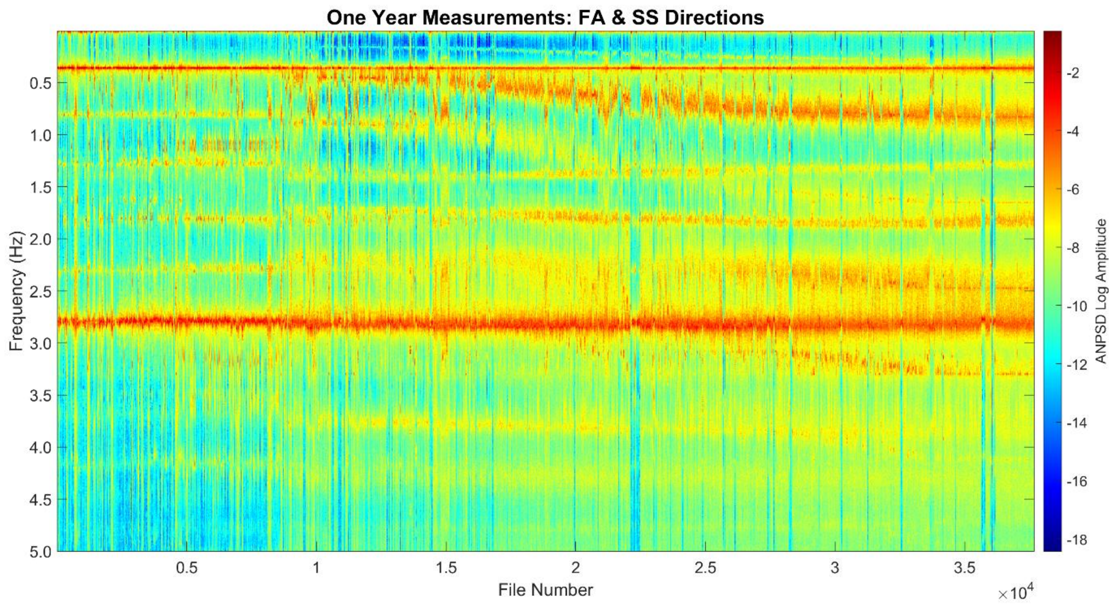

Figure 26 - Colour Map for one-year measurements, considering both directions, ordered by rotor speed.

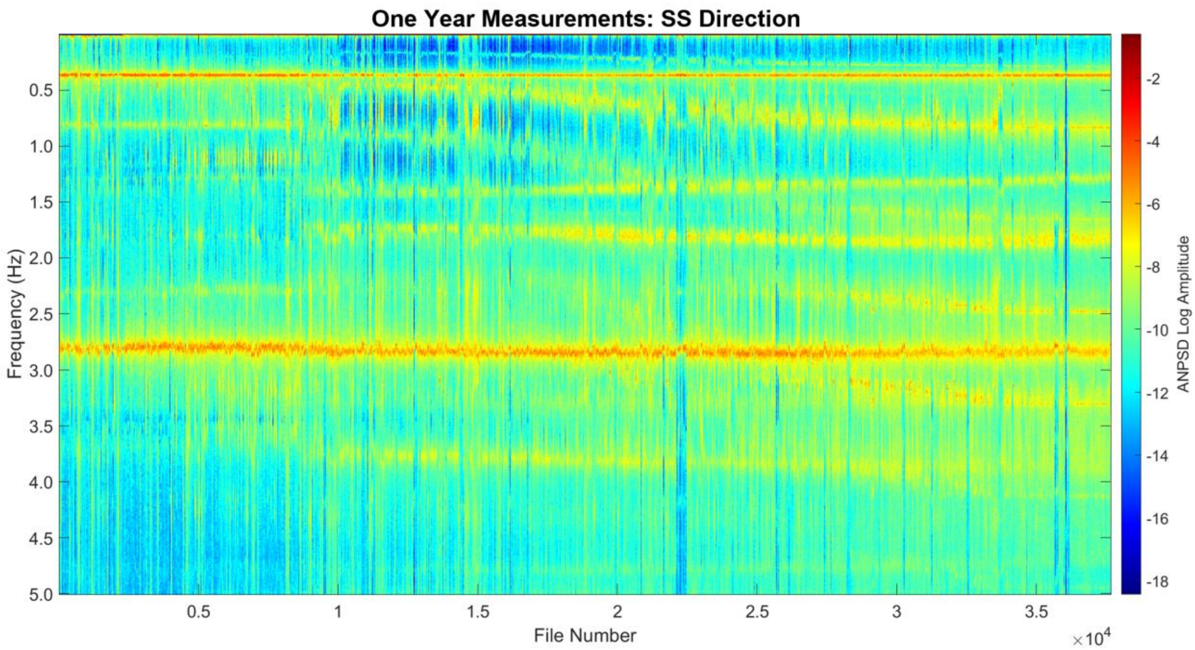

Figure 27 - Colour Map for one-year measurements, considering the side-side direction, ordered by rotor speed.

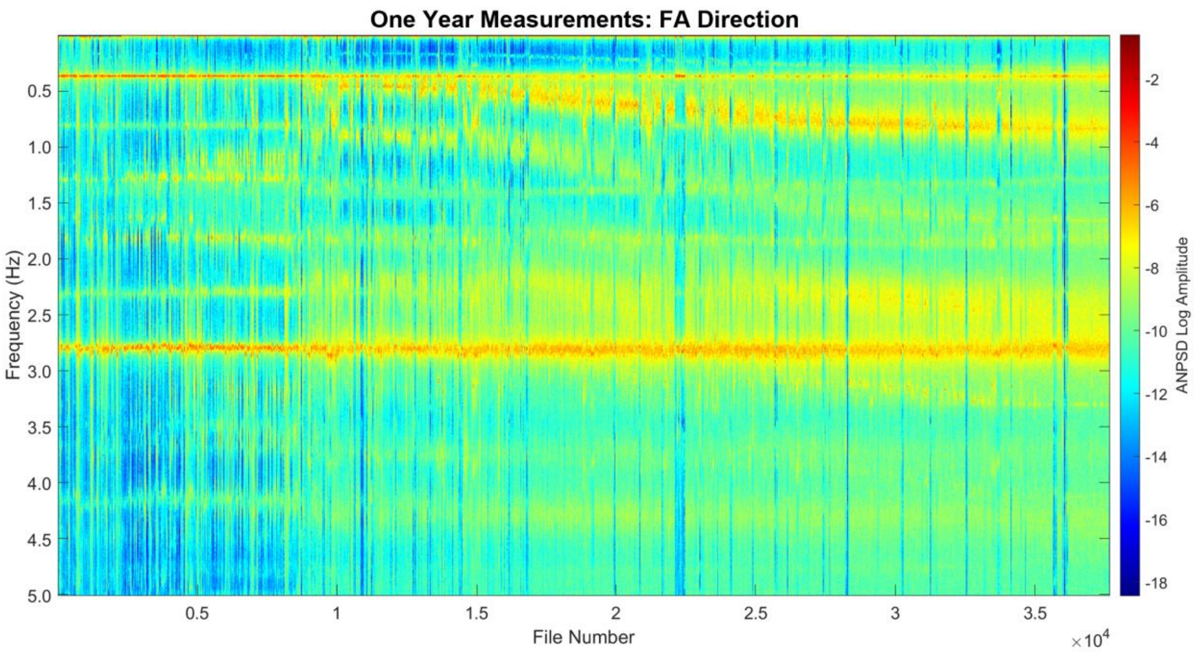

Figure 28 - Colour Map for one-year measurements, considering the fore-aft direction, ordered by rotor speed.

Figure 29 and Figure 30 present, respectively, two examples of stabilization diagrams, for parked and rotational conditions, both obtained with a maximum model order of 76. The coloured grouping of poles represents the modes defined by the method, while the pink crosses identify the poles whose modal properties represent that mode and the red function is the modal model for the higher model order.

In operation, it is evident a higher variance in the modal model graph and the number of clusters identified is also larger due to the poles' dispersion. Whereas, in parked conditions, the stabilization diagram is cleaner and more stable.

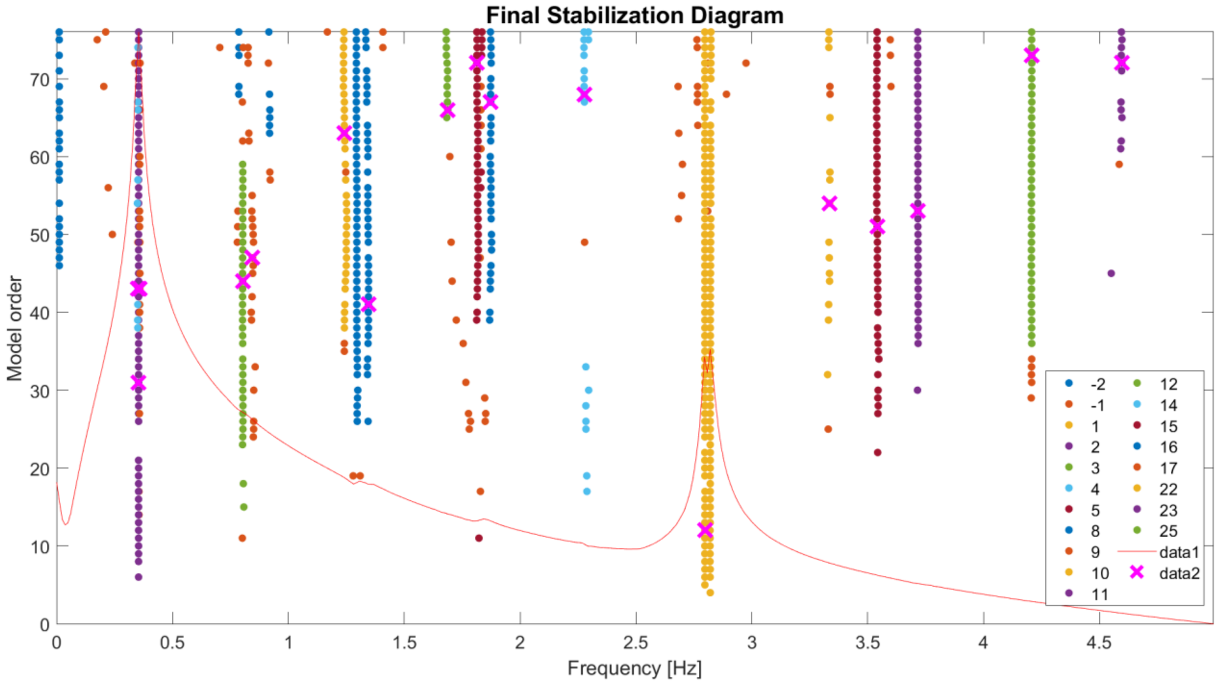

Figure 29 - Stabilization Diagram for a time series with the wind turbine in parked conditions.

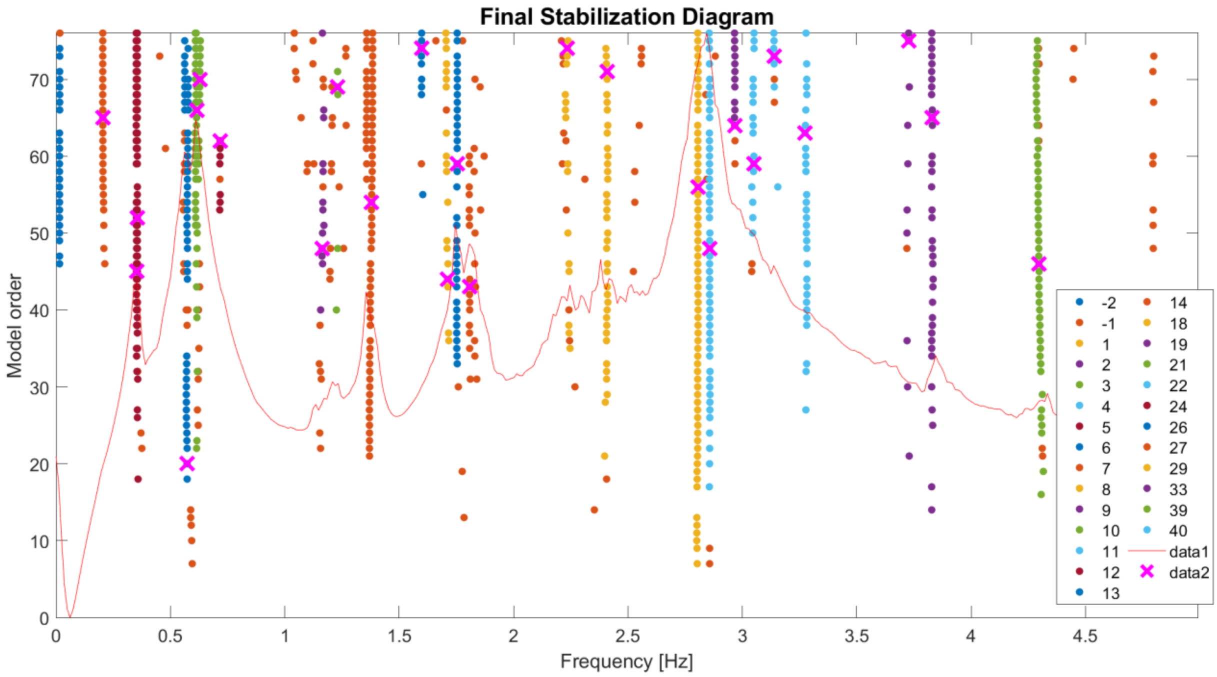

Figure 30 - Stabilization Diagram for a time series with 12 rpm of rotor speed.

5

AUTOMATED OPERATIONAL MODAL ANALYSIS METHODOLOGY

5.1. AUTOMATED MODAL PARAMETER SELECTION

The Automated Modal Parameter Selection (AMPS) is an intelligent rule-based procedure that selects poles in a stabilization diagram faster and more consistently than the manual process done by different levels of expert engineers, as reported in [13].

Figure 31 explicit the AMPS methodology, composed by three steps. First, a clustering technique, DBSCAN, is applied to discard noise points and to aggregate the poles with similar characteristics, namely damping ratios and natural frequencies. Lastly, two verification steps are introduced to identify and evaluate the potential vibration modes. The first step aggregates clusters related to the same mode, an important application to complex systems. The last step discards spurious or numerical modes based on each cluster modal parameters and contribution to the final modal model synthesis.

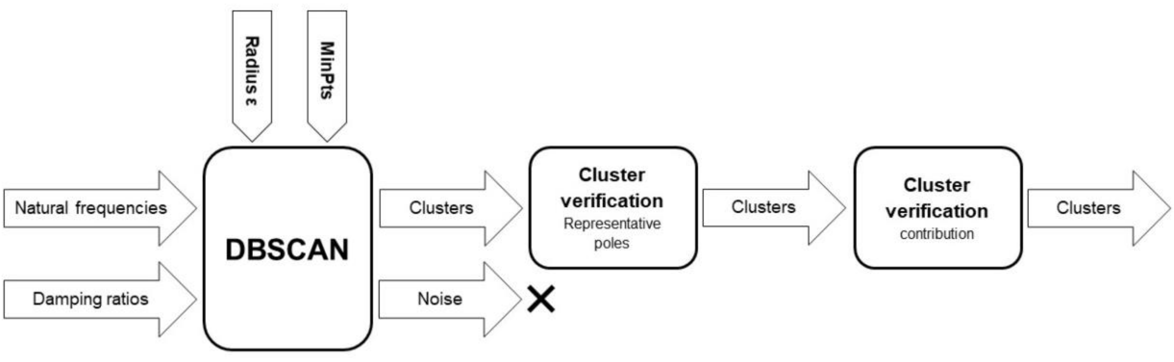

Figure 31 - Automated Modal Parameter Selection [13].

5.1.1. DBSCAN Clustering

The DBSCAN clustering algorithm is utilized to define the stabilization diagram initial clusters and, as presented in Section 2.2, is based in a distance criterion.

In the present work, the distance depends on the pole's modal parameters: frequency and damping ratio. Equation (15) presents the distance calculation between two points (p_i and p_j) in a stabilization diagram with N_p points. The distance criterion is defined as the sum of the absolute differences normalized in frequency and damping due to the magnitude discrepancy between the two inputs.

$$d(p_i, p_j) = d_f(p_i, p_j) + d_\xi(p_i, p_j) = \frac{\left|f_{p_i} - f_{p_j}\right|}{f_{p_i}} + \frac{\left|\xi_{p_i} - \xi_{p_j}\right|}{\xi_{p_i}}; i, j \in \{1, 2, \dots, N_p\} \tag{15}$$

To ensure the versatility of the method, the input values are carefully selected. The minimum number of points ($minpts$) to define a cluster is one-sixteenth (1/16) of the model size, inferiorly limited to 3. This option allows the fit between model and cluster size, while the smaller threshold eases the smaller clusters grouping [14].

The stability criteria allow 1% frequency variation and 5% damping variation for the radius definition used to select the stable poles in the stabilization diagram, resulting in a radius (ε) of 0.06 [13]. In fact, one pole can be associated to the cluster even though its frequency variation is above 1% if the total discrepancy is inferior to 6%.

5.1.2. First Cluster Verification Step

For complex structures whose stabilization diagrams are defined for high model orders, the damping ratios for the same mode may vary more than the permitted by the stability criteria, leading to a mode separation in different clusters. This first cluster verification step aims to assemble different clusters that represent the same mode, maintaining the representative characteristics of the primary cluster (with higher number of poles) and rejecting the secondary representative modes.

To enter this first verification step, the distance between the clusters defined in DBSCAN clustering phase are computed according to equations (16) and (17). Similar clusters are the ones whose representative poles (rp) frequency variation is inferior to 2% and, simultaneously, the MAC between the two is equal or superior to 80%.

$$d_f(rp_i) = \frac{\left|f_{rp_i} - f_{rp_j}\right|}{f_{rp_i}}; i, j \in \{1, 2, \dots, N_c\} \tag{16}$$

$$d_{MAC(L)}(rp_i) = 1 - \frac{\left|\gamma_{rp_i}\gamma_{rp_j}\right|^2}{(\gamma_{rp_i}\gamma_{rp_i})(\gamma_{rp_j}\gamma_{rp_j})}; i, j \in \{1, 2, \dots, N_c\} \tag{17}$$

The wind turbine is a special structure that often presents cross-frequency structural modes due to their small mass and stiffness asymmetry. To ensure theses modes are separated during the AMPS procedure, the first cluster verification was improved with three conditions.

The first condition relies in a poles number comparison and the next two conditions stand for the modal order coincidence. Figure 32 presents a procedure scheme and the conditions are further explained:

1. If the secondary mode has more than 50% of the primary cluster poles number, it proceeds to the next condition, otherwise the clusters are assembled;
2. If the model orders of the poles that form the two cluster do not coincide, the clusters are gathered, contrarily it pursues the third condition;
3. Analysing the primary cluster, if more than half of the poles number coincide in terms of model order with the secondary cluster, they remain separate, if not they are merged, maintaining the primary cluster representative characteristics as the representative of the new cluster.

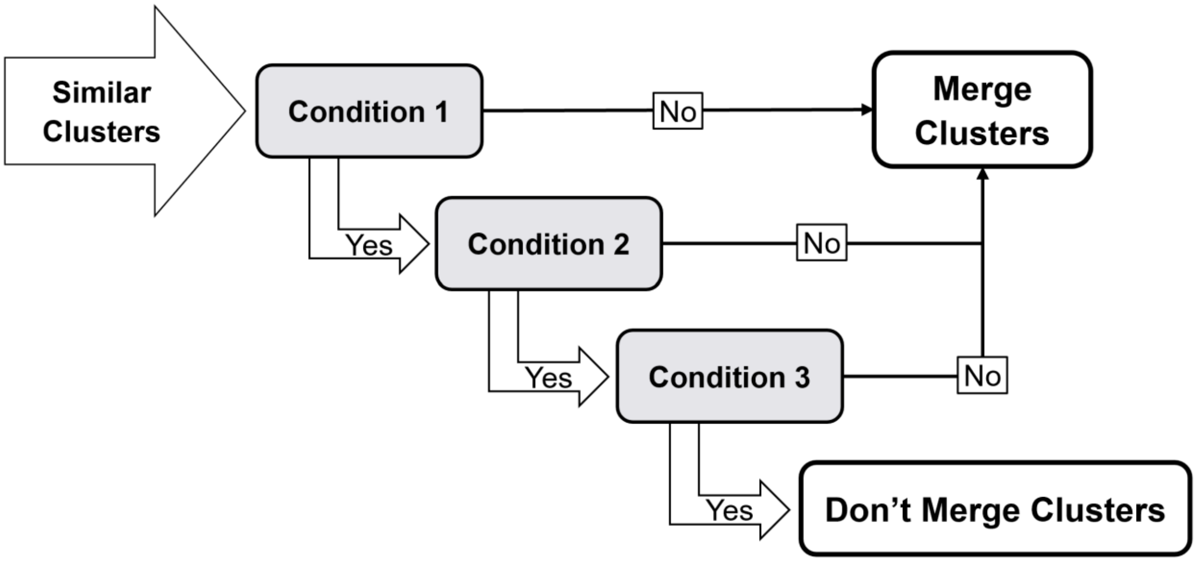

Figure 32 - Schematic First Verification Step Presentation.

5.1.3. Second Cluster Verification Step

The second cluster verification step aims to eliminate the clusters associated to spurious or numerical modes. This exists due to measurement problems, whose noise generated in the collected data originates spurious modes in the response spectrum, and/or due to an over-selection of the model order that leads to a fitting polynomial sensitive to minor dynamics that don’t derive form the physical structural behaviour of the system.

An in-house method was applied to determine the modes contribution with respect to the modal model synthesis. Each mode contribution is associated with the representative pole of its cluster [14].

This last Automated Modal Parameter Selection step is divided in two parts: first the reference clusters are selected based on the representative poles that contribute the most to the frequency-domain response and then the minimum contribution and maximum damping ratio are defined amongst the selected modal parameters. Finally, a three-phase conditioning, depicted in Figure 33, is performed to classify the clusters as dubious or physical. The three conditions are presented hereafter:

1. If the cluster damping exceeds ten times the damping reference value, the cluster is immediately classified as spurious, otherwise it proceeds for the second condition;
2. The minimum contribution allowed is determined considering a standard value of 2%: if the minimum contribution is superior to the standard, the minimum contribution allowed is defined as minimum contribution minus 0.01, otherwise it is defined as half of the minimum contribution. If the cluster contribution is inferior to the minimum contribution allowed, the third condition follows, otherwise the cluster is classified as physical;
3. Lastly, if the cluster poles number is smaller than 85% of the minimum number of poles identified among the reference clusters or inferior to the double of the $minpts$ defined in the DBSCAN clustering phase, the mode is classified as spurious and eliminated.

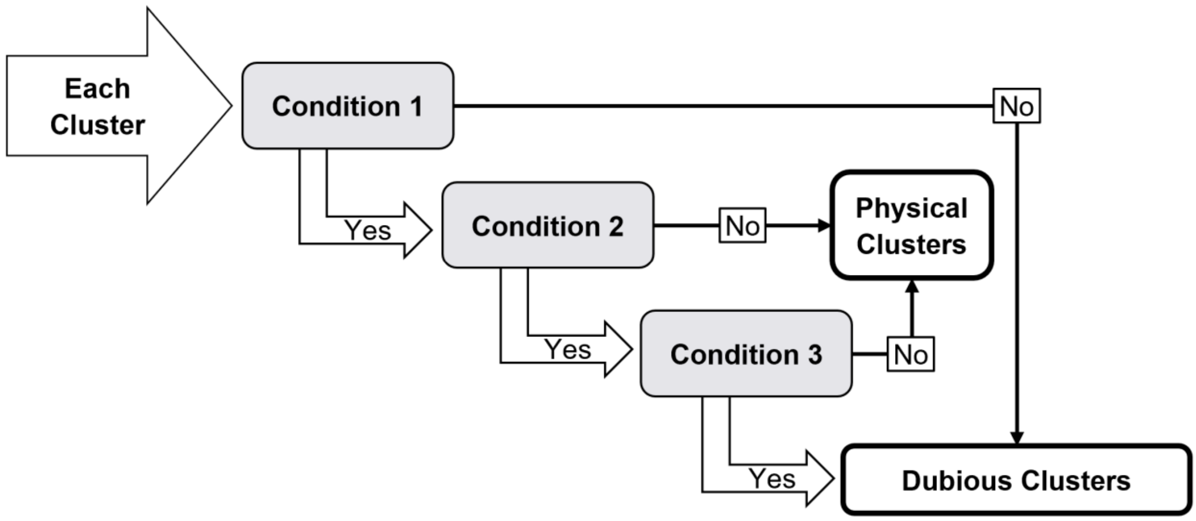

Figure 33 - Schematic Presentation of the Three-phase Conditioning from the Second Verification Step.

5.2. AUTOMATED MODAL TRACKING

The final step of Automated Modal Analysis (AMA) is the modal tracking, occurring after estimating the modal parameters, performed by the MPE (briefly described in Section 2.1.2), and after the final clusters definition, which is executed by the AMPS (presented in Section 5.1). The final stabilization diagram and set of resonance modes that define the structures dynamic behaviour are the AMPS output and the input to perform modal tracking. Figure 34 presents the framework of modal tracking in the AMA process.

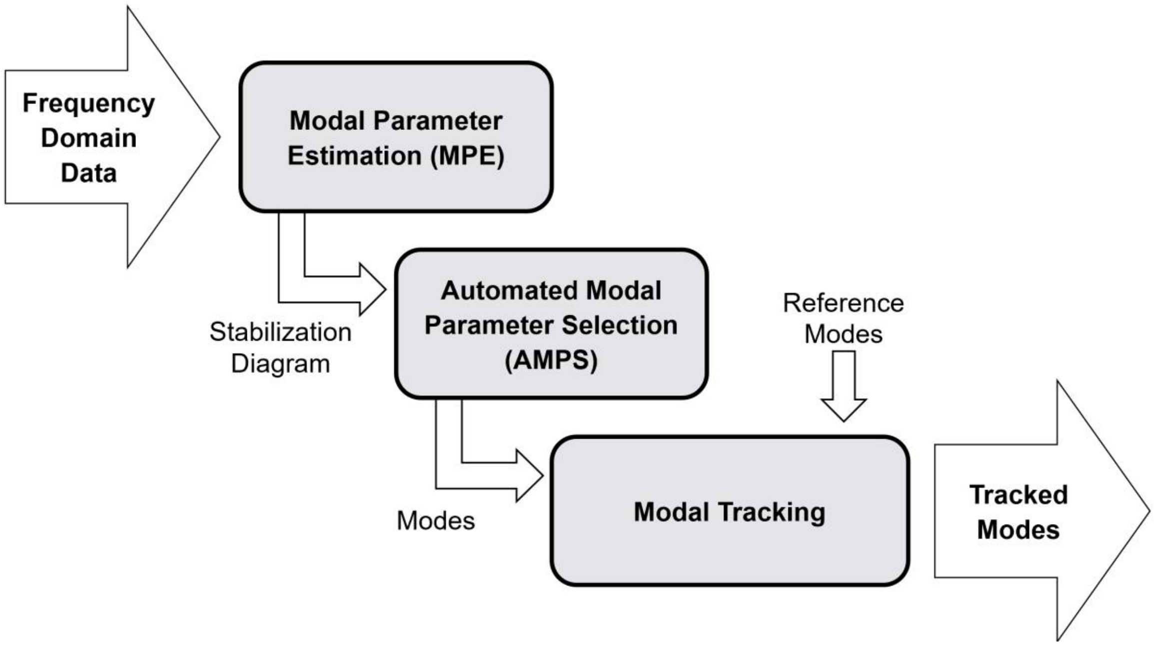

Figure 34 - AMA Process for Long-term Monitoring.

Modal tracking is the process to evaluate the modal parameters similarity between reference modes, that might be actualized over time, and resonance modes associated to a certain measurement. The correlation between modes is relevant in long-term monitoring processes to identify alterations in the modal parameters, that might be associated with different operating conditions, seasonal aspects (temperature fluctuation, ice formation in the structure, among others), damage or others.

In the case of wind turbines, there are modes with very similar natural frequencies and damping, enhancing the difficulty to identify them both through the previous procedures, decreasing the success of modal tracking. The yaw angle variation combined with asymmetric soil and structure conditions leads to alterations in the modal parameters that may lead to crossing frequencies. [12]

The modes tracking is performed by determining the distance between the modal parameters, namely frequencies and mode shapes. For the two parameters, the distance is determined comparing a set of resonance modes resulting from a certain measurement, *mode 1*, and a group of reference modes to be tracked over time, *mode 2*. The distances formulas are presented in equations (18) and (19).

If the distances are within a threshold, the measurement mode is associated with the closer reference mode. The thresholds definition depends on the structure type, on its dynamic behaviour and on the number of measured DOFs. This last aspect is related to the spatial aliasing phenomenon, occurring when the measured spatial sampling data is insufficient to characterize adequately the structure dynamics [56].

$$d_{freq} = \frac{|f_{m_1} - f_{m_2}|}{f_{m_1}} \tag{18}$$

$$d_{MAC} = 1 - \frac{|\varphi_{m_1}\varphi_{m_2}|^2}{(\varphi_{m_1}\varphi_{m_1})(\varphi_{m_2}\varphi_{m_2})} \tag{19}$$

5.2.1. Fixed Reference Modes

For the developed work, a 3.5% frequency variation is the limit imposed and the minimum MAC between the reference mode and the resonance mode is 70%. The final condition, given by Equation (20), results in a maximum allowed distance of 33.5%. Note that, the discrepancies can be distributed differently, respecting the defined criteria of 0.335 total distance limit.

$$d_{TOTAL} = d_{freq} + d_{MAC} \leq 0.335 \tag{20}$$

The detected clusters representative poles in a certain stabilization diagram, that verify the tracking condition are classified as similar poles. If there is only one similar pole, it is assigned to the reference mode, however if more than one similar pole is identified, the one with smaller total distance is tracked.

Random measurement setups were investigated and the plainer mode shapes corresponding to the anticipated were designated to establish the reference, presented in Figure 35.

The MAC matrix correlating the reference mode shapes is represented in Figure 36. Analysing the matrix, the mode pairs with the highest MAC values exhibit very similar mode shapes, being associated with the same direction. The modes 3FA and 3SS*, whose MAC value is 78%, have the largest collinearity, which can be explained by the reduced number of measured system DOFs, insufficient to accurately define the mode shapes, corresponding to the spatial aliasing phenomenon.

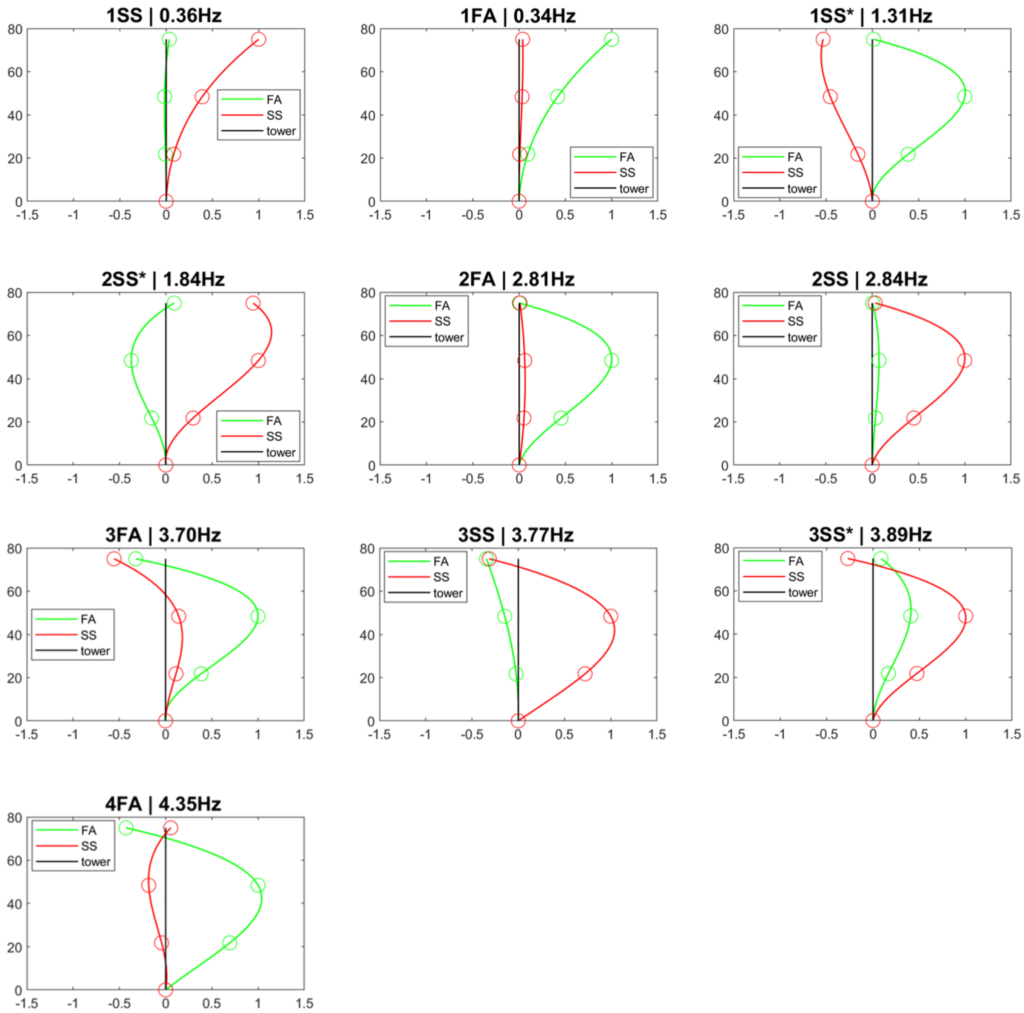

Figure 35 – Fixed reference frequencies and mode shapes.

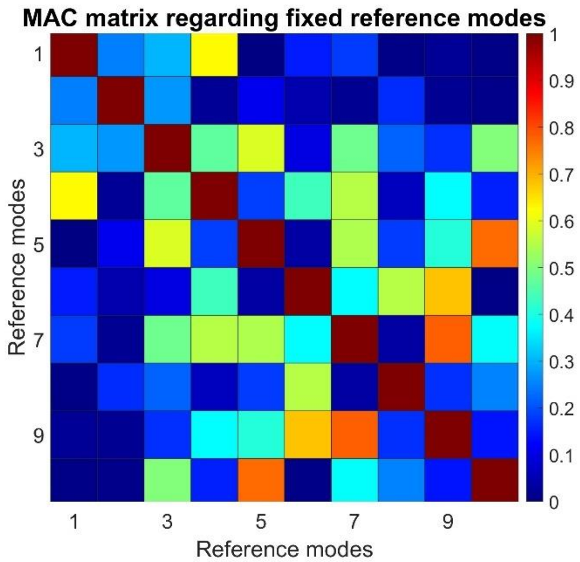

Figure 36 - MAC matrix involving the fixed reference modes.

5.2.2. Adaptative Reference Modes

The methodology implemented to perform modal tracking with an adaptative reference implies the initial definition of certain parameters: the number of previous poles to study to select the new reference (*n_prev*) and the initial reference, namely frequencies and mode shapes for all the modes to be tracked.

This process implies a tracking as presented in subsection 5.2.1 until the number of poles tracked equals the number of previous poles to study. After the *n_prev* poles frequencies are averaged, the new reference is selected as the one whose damped frequency is nearest to the mean value.

The tracking process follows the same procedure as for fixed reference modes and, whenever a new pole is tracked, this iterative process to select the new reference is repeated.

To select the initial reference different measurement setups, whose rotor speed is about 9 rpm with a 3.33% variation allowed, were analysed. This value was chosen, since from there on, the power output suffers a significant increase, as related in Figure 23. The modes whose mode shapes were clearer and analogous to the expected were selected to create the initial reference, shown in Figure 37, leading to frequency discrepancies when compared to the reference modes in Figure 35.

Figure 38 represents the MAC matrix among the initial reference mode shapes. Analysing the matrix, the pairs of modes with highest MAC value are related to the same direction and present very similar mode shapes. Modes 2SS and 3SS*, whose MAC value is 86%, have the largest collinearity.

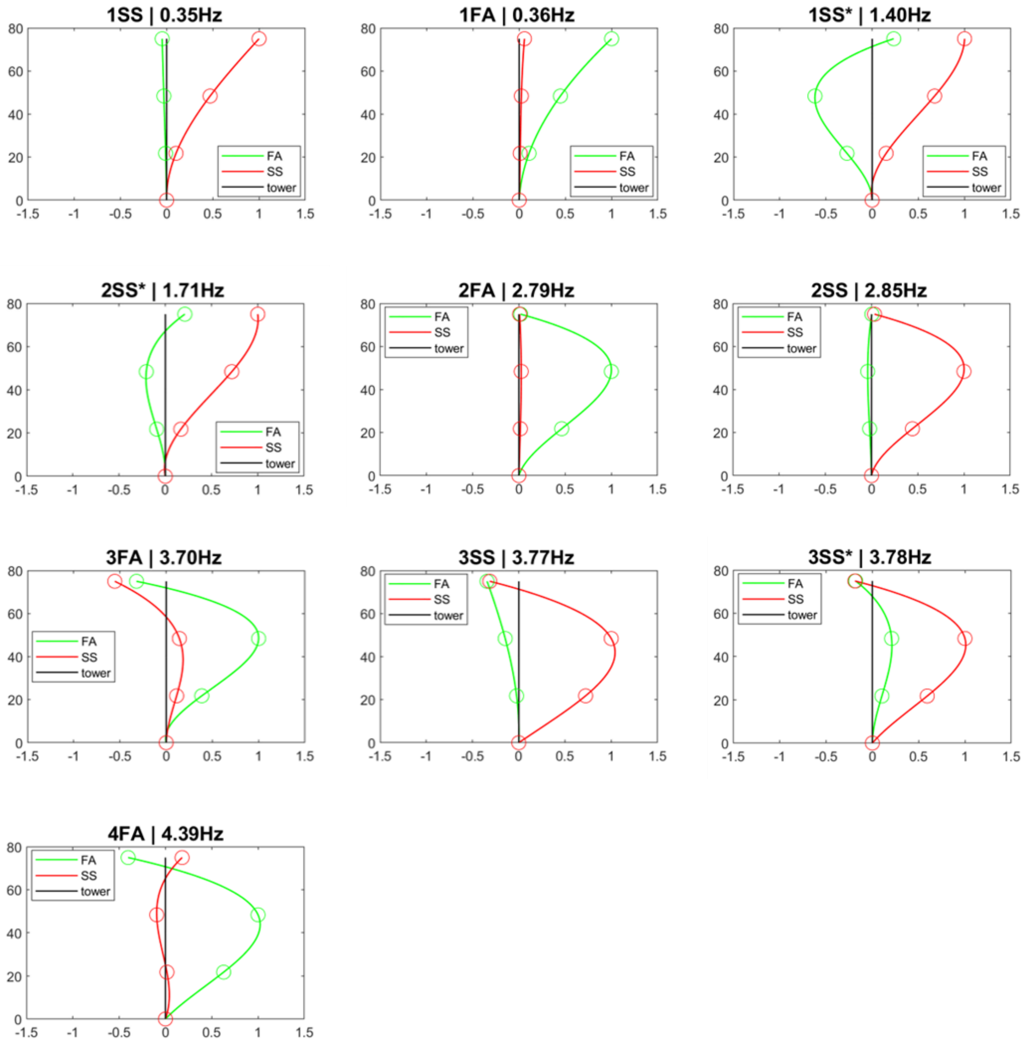

Figure 37 – Initial adaptative reference frequencies and mode shapes.

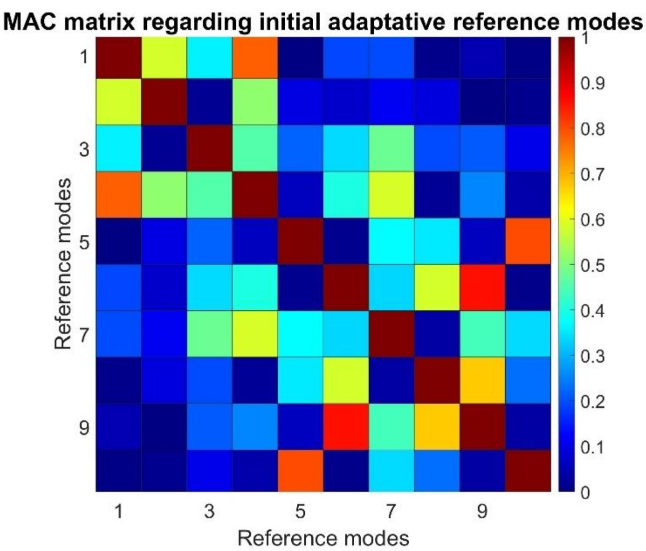

Figure 38 - MAC matrix involving the adaptative reference modes.

6
WIND TURBINE MONITORING

6.1. AUTOMATED MODAL PARAMETER SELECTION

The AMPS procedure was implemented to estimate the modal parameters with respect to all the measured data. In this section the cluster verification steps results are presented for two different time series recorded.

The MPE phase is antecedent to the AMPS. In the first one, the PolyMAX was used to estimate the modal parameters and 4096 time lags were considered, associated with a 1% exponential window to reduce leakage effects and the influence of larger time lags, whose variance is higher [17]. The method was applied to a frequency range between 0 and 5 Hz and for a maximum model order of 76. Each stabilization diagram was derived with these considerations for 10-minute acceleration series.

6.1.1. FIRST CLUSTER VERIFICATION STEP

Figure 39 presents a stabilization diagram after the MPE phase and before the DBSCAN clustering phase, the AMPS first step.

Figure 40 presents the same stabilization diagram after the AMPS procedure appliance. The modes within the drawn boxes are kept separated in the first cluster verification step. This result is relevant once these mean frequencies (0.35 & $3.70\ Hz$) are associated to pairs of structural modes, closely spaced in the frequency domain.

The poles with the -1 label were classified as spurious by the DBSCAN clustering algorithm and the ones with positive number identifier correspond to clusters formed through first cluster verification step implementation after the DBSCAN was utilized. The pink crosses point each cluster’s reference pole.

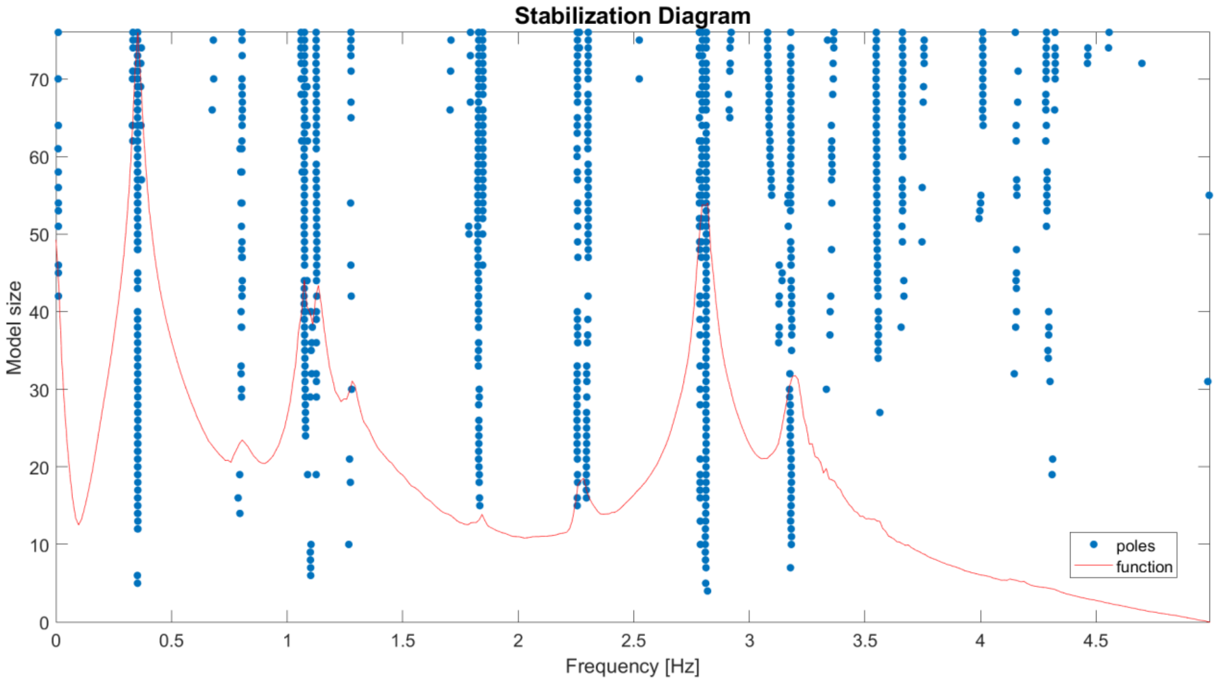

Figure 39 - Stabilization Diagram after PolyMAX procedure and before DBSCAN stage.

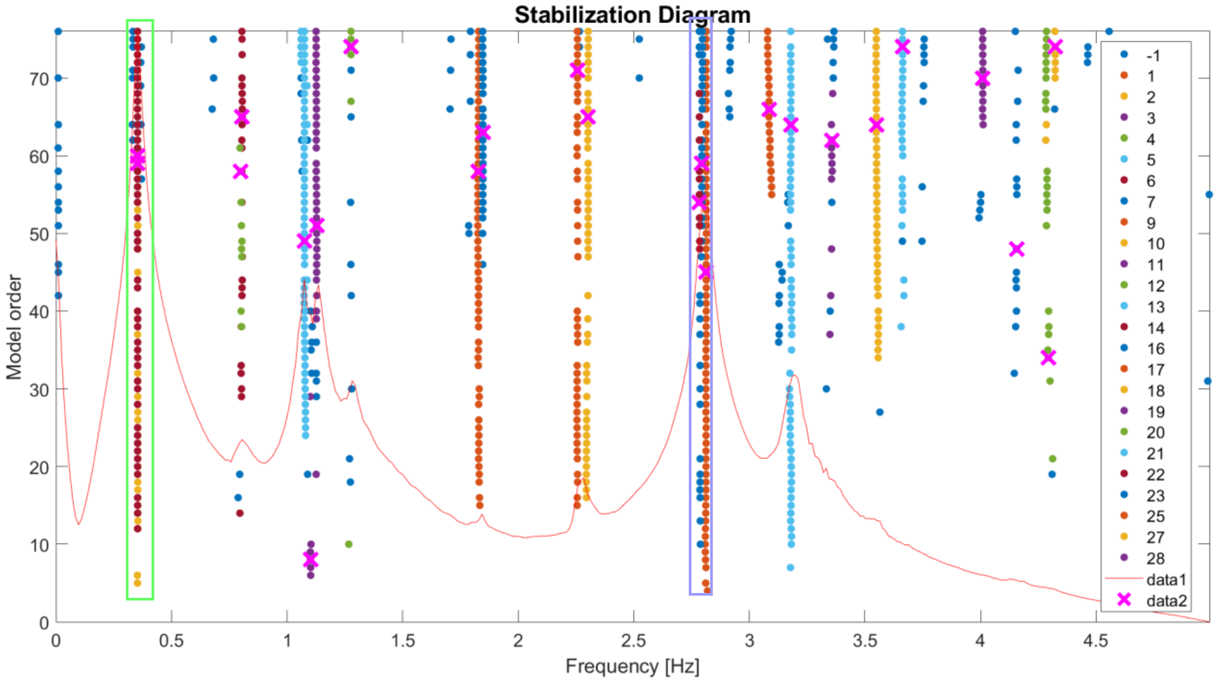

Figure 40 - Stabilization Diagram with Modes Separated in First Verification Step.

6.1.2. Second Cluster Verification Step

The stabilization diagram represented in Figure 41 is obtained through the modal parameter estimation methodology.

Subsequently, the AMPS methodology is applied and the final stabilization diagram is introduced in Figure 42. Analogously to the Figure 40 legend, the poles labelled as -1 were classified as numerical by the DBSCAN and the poles with positive integer identifiers are associated to the same clusters after the first cluster verification step, while the pink crosses signalize the reference pole of each cluster. The poles identified with -2 represent numerical clusters and were defined after passing the second cluster verification step.

The modes within the boxes were deleted through the second cluster verification step: the two modes in the red box are eliminated in the first condition and the ones inside the blue boxes were eliminated after verifying the second and the third conditions. The calculations and explanation for their discard are further presented.

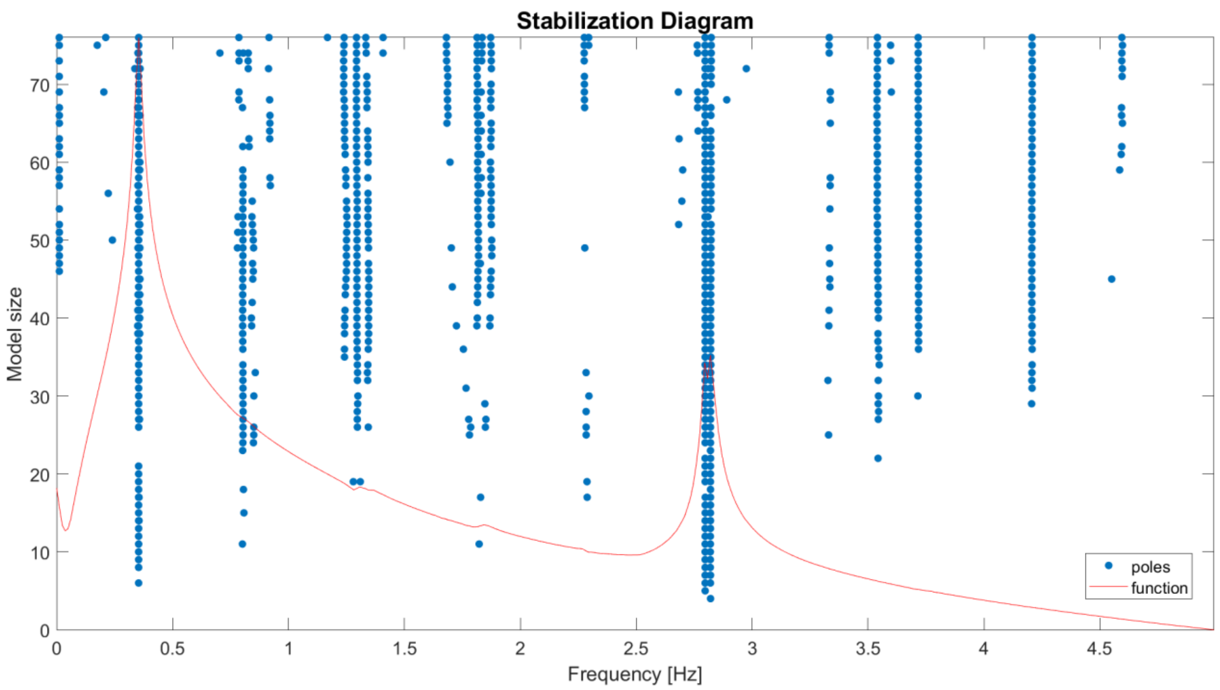

Figure 41 - Stabilization Diagram after PolyMAX procedure and before DBSCAN stage.

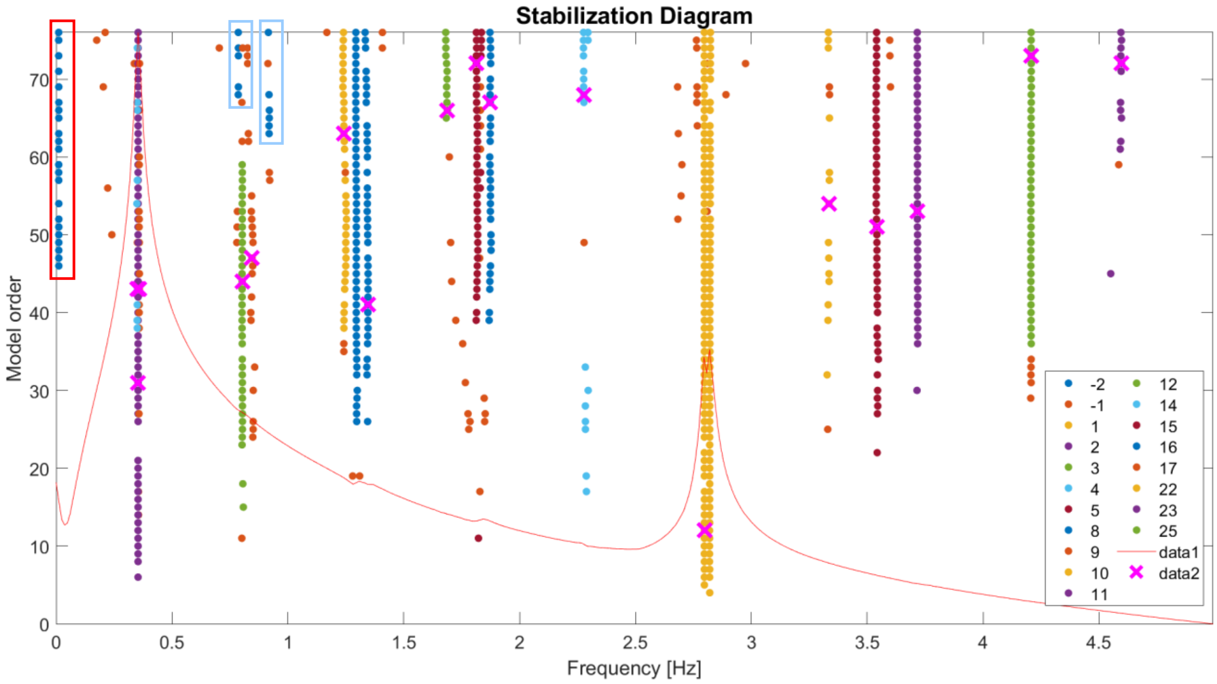

Figure 42 - Stabilization Diagram with selection of modes to be discarded within the red and blue boxes.

There are two modes inside the red box, for whom the first condition is not met: the modes representative damping is inferior to the maximum damping allowed.

$$f = 0.01Hz: \xi = 98.75\% > \xi_{max} = 27.09\%$$

$$f = 0.01Hz: \xi = 98.95\% > \xi_{max} = 27.09\%$$

The two modes inside the blue boxes respect the first condition in the second verification step, however their contribution to the response measured is inferior to the minimum contribution allowed ($MinCont$), followed by a third condition non-verification. Therefore, both modes are classified as spurious and are eliminated. The results for the 0.79Hz mode are the following:

$$1^{st} Condition: \xi = 1.71\% < \xi_{max} = 27.09\%$$

$$2^{nd} Condition: cont = 0.0336 < MinCont = 0.0351$$

$$3^{rd} Condition: poles = 5 < \min(0.85 * 66; 2 * 5) = 10$$

For the 0.92Hz mode:

$$1^{st} Condition: \xi = 1.84\% < \xi_{max} = 27.09\%$$

$$2^{nd} Condition: cont = 0.0331 < MinCont = 0.0351$$

$$3^{rd} Condition: poles = 6 < \min(0.85 * 66; 2 * 5) = 10$$

6.2. Automated Modal Tracking

In Figure 43 are shown the AMPS results for all the February measurement data. The data series are ordered per rotor speed, represented by the red alignment, to evidence their effect on the natural frequencies of the identified modes.

Modes 3 and 4, associated to 1.31 and 1.84 Hz frequencies, are highly affected by the rotor speed, not being identified through the AMPS procedure when the rotor is parked. While the first referred mode registers a frequency decrease with increasing rotational speed, the 1.84 Hz mode has the opposite tendency. The ninth mode, at 3.78Hz, is also affected by the rotational frequency.

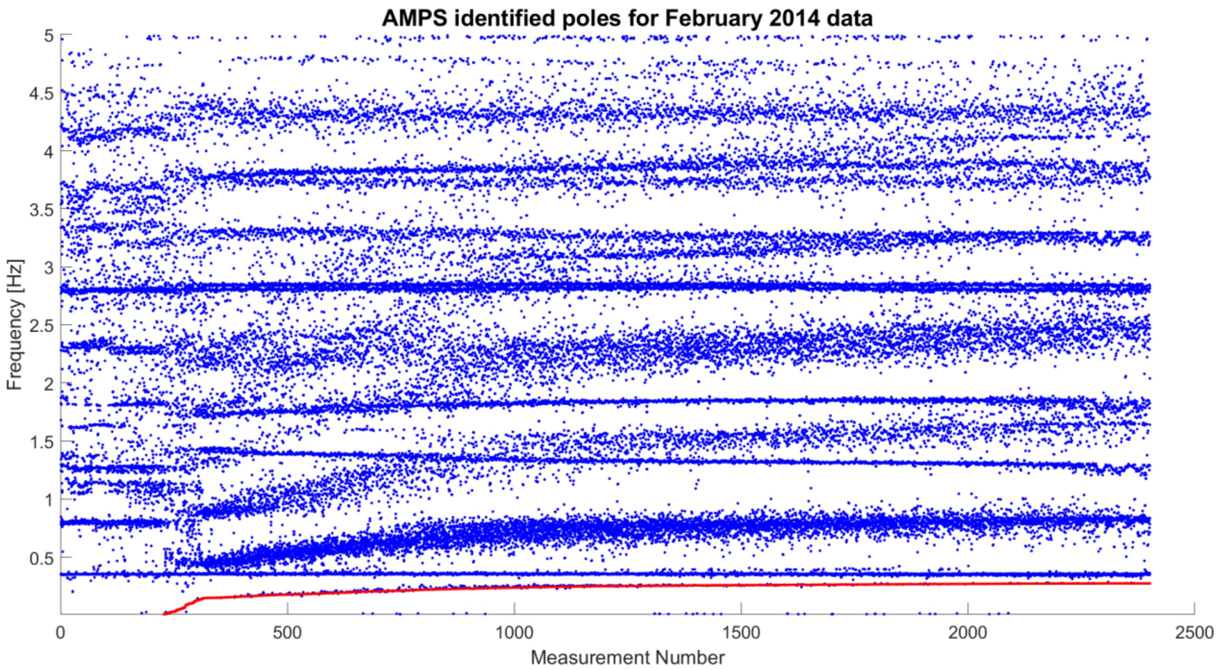

Figure 43 - AMPS results for February measurement data, ordered for increasing rotor speed (represented graphically by the red line).

6.2.1. Fixed Reference Modes

The automated modal tracking results for February, regarding fixed reference modes, are enhanced in Figure 44, and Table 1 presents the tracking success rate, the frequency average, standard deviation and variation (Equation (21)), and the average and standard deviation of MAC amongst all the tracked modes for a certain reference mode. The MAC value, for each tracked mode is computed with that mode fixed reference.

$$\Delta f = \frac{f_{max} - f_{min}}{\bar{f}} \tag{21}$$

The mode 3SS is the least tracked in this month, being registered in less than 10% of the setups, while modes 1FA and 3FA were tracked in 18%. All the other modes have success rates superior to 50%, except for the 1SS* with 31% success rate. The average MAC is generally above 85% and the frequency variation is below 7%. These results indicate high similarity amongst the tracked modes with respect with the reference modes, leading to high quality results despite the lower success rate encountered for some of the tracked modes.

Figure 45 presents the tracked damping ratios organized per frequency and per increasing rotor speed. The modes 1FA and 1SS have higher damping ratio values and, from Figure 45 b), this parameter value increases as the rotor speed enhances. In theory, the aerodynamic damping contribution for mode 1FA is uniquely enhanced by increasing wind speed, which is directly correlated with rising rotor speed. This suggests that the identification of certain modes may be inaccurate.

Figure 46 introduces the MAC evolution for the tracked poles associated to the modes 1SS, 2SS*, 2SS and 4FA.

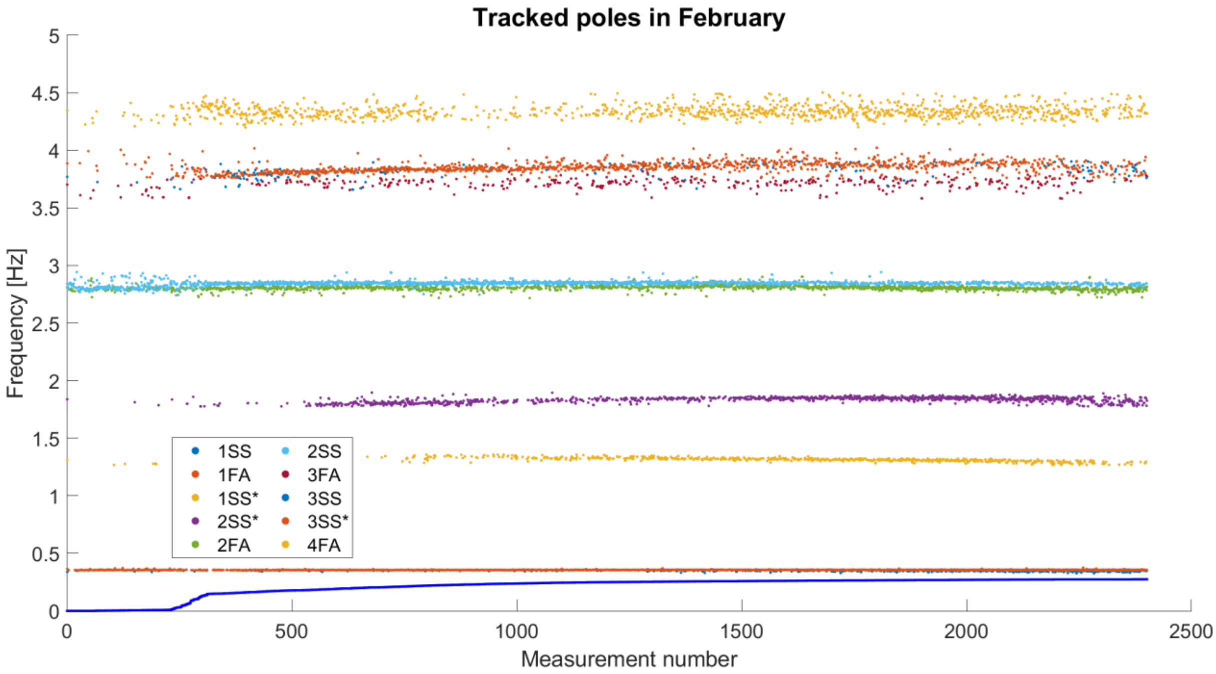

Figure 44 - Tracked modes in February, with fixed reference, ordered for increasing rotor speed.

Table 1 - Automated Modal Tracking Results for February, considering a fixed reference.

Mode	Success Rate (%)	$\bar{f}(Hz)$	$\Delta f(\%)$	f_{std}	$\overline{MAC}$	MAC_{std}
1SS	89.963	0.356	6.572	0.002	0.937	0.061
1FA	17.493	0.345	6.806	0.004	0.929	0.070
1SS*	31.404	1.315	6.892	0.017	0.821	0.074
2SS*	55.060	1.833	6.526	0.023	0.888	0.075
2FA	78.467	2.805	6.624	0.019	0.922	0.076
2SS	76.926	2.844	6.966	0.020	0.924	0.076
3FA	17.993	3.715	6.859	0.046	0.810	0.076
3SS	9.579	3.818	6.483	0.055	0.776	0.062
3SS*	58.601	3.854	6.924	0.044	0.845	0.075
4FA	54.394	4.339	6.986	0.055	0.872	0.077

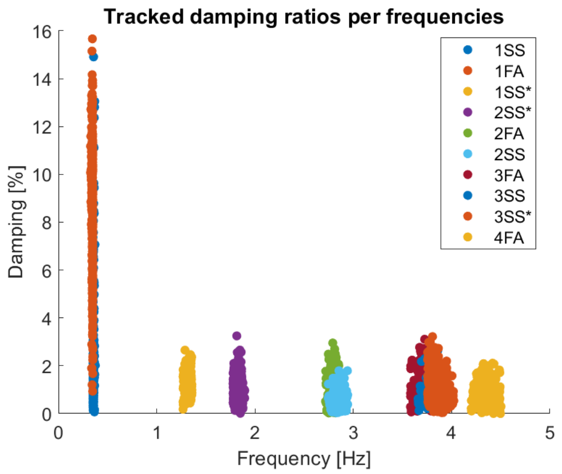

a)

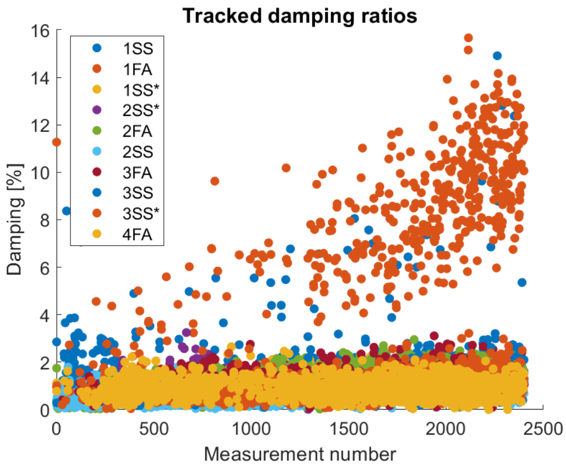

b)

Figure 45 - Damping evolution, considering fixed reference: a) per frequency and b) per measurement, ordered by increasing rotor speed.

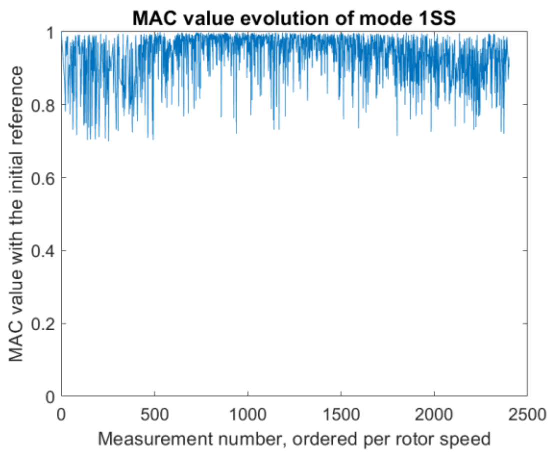

a)

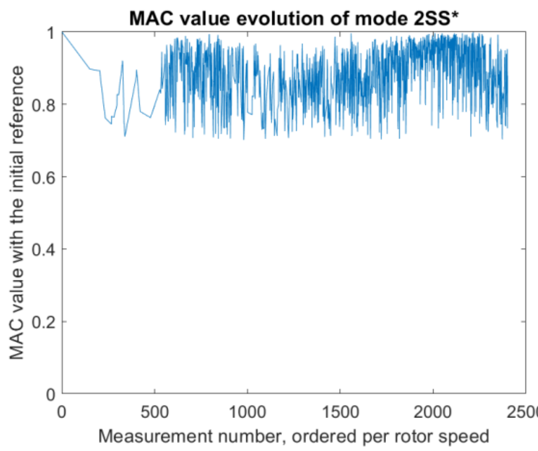

b)

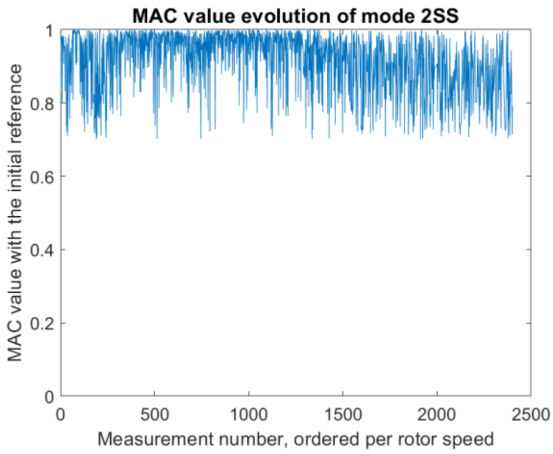

c)

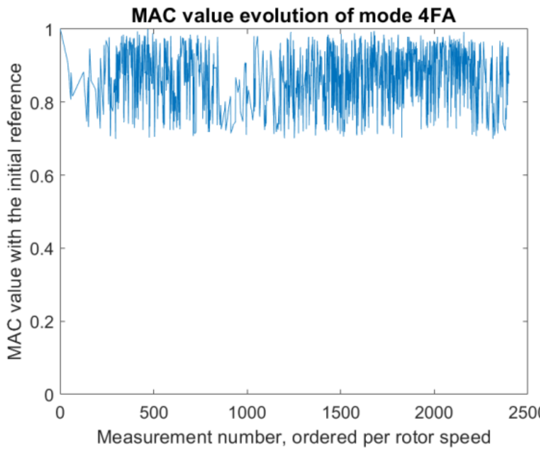

d)

Figure 46 - MAC value evolution, considering fixed reference, of modes: a) 1SS, b) 2SS*, c) 2SS and d) 4FA.

6.2.2. Adaptative Reference Modes

Figure 47 illustrates the automated modal tracking results for February concerning adaptative reference modes with *n_prev* =100, introduced in subsection 5.2.2. Table 2 displays the statistical results, namely the tracking success rate, the average frequency and variation, and the average MAC value for all modes tracked relative to a specific reference mode.

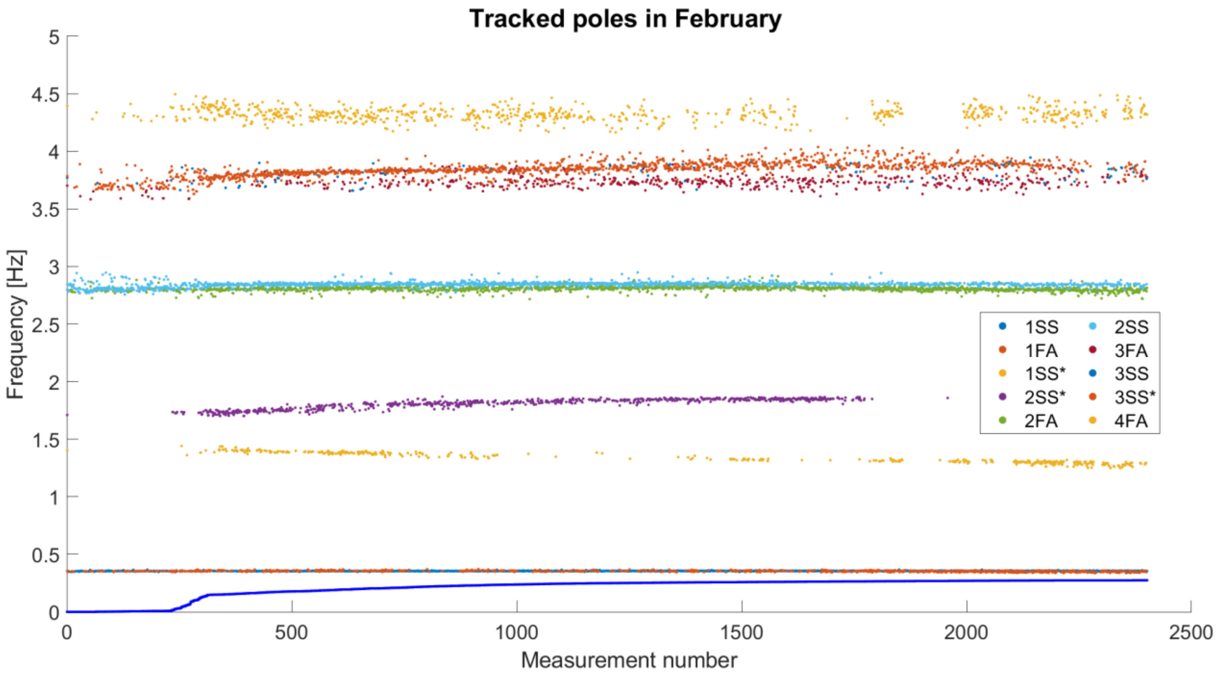

Figure 47 - Tracked modes in February, with adaptative reference, ordered for increasing rotor rotational speed.

The tracking procedure success rates are inferior to 50% in half of the modes: 3SS, 1SS*, 3FA, 2SS*, 4FA and 1FA, ordered with crescent tracking success. The first two modes on the list are represented in less than 20% of the measurement data setups.

The metrics analysed are more scattered for the adaptative reference when comparing with the fix reference, since the frequency variation diverge from mode to mode and the average MAC value fluctuates more, reaching values inferior to 50% for the 2SS* mode.

The mode 1SS presents the best results: the greatest success rate of approximately 88%, the lowest frequency variation of 6.5% and an average MAC between the tracked modes of 0.93. Despite this high value, the MAC reaches values inferior to 0.5 during the tracking process, as seen in Figure 49 a).

The minimal success rate is less than 6% and is linked to mode 3SS, whose mean MAC is close to 75%. Despite 35% of the measured setups registered the mode 2SS*, the average MAC value between those and the initially defined reference is 47%. The highest frequency variation is almost 15% for the mode 1SS*, with low representativeness in the data and with an average MAC of 0.8.

Figure 49 d) represents the MAC value evolution for the tracked modes associated with mode 4FA and, from 0 to 400 measurement setups (when the rotor speed is 8.8 rpm) the mode is almost not present, indicating this mode is excited by the rotor dynamics. From there on, the average MAC value has a decrescent tendency until close to 14.3 rpm (dataset 1000), where MAC values inferior to 0.1 are registered. Afterwards, a crescent tendency is found, even though with highly scattered values. The high MAC standard deviation of 27% is the statistical indicator for the perceptible sparsity behaviour. When comparing these results with the previous subchapter ones (Figure 46 d)), the abrupt decrease described is associated to an area with scarce modes tracked.

The 2SS* modes considered in the fixed reference and initial adaptative reference present a MAC value of 0.9. Given the mode shapes consistency observed in Figure 46 b), for fixed reference tracking, the expected was to obtain a similar record with the adaptative reference. However, Figure 49 b) indicates the procedure got lost in the second iteration where the MAC decreased to 0.26 with respect to the initial reference. Therefore, the adaptative reference couldn't return to the initial mode shape what is also confirmed for the moderate MAC value standard deviation associated with an average MAC inferior to 50% (Table 2). This observation might also indicate that the initial reference mode was not accurately selected.

The mode 2SS registers similar results to the observed for 2SS*, including approximate standard deviation values, despite the higher average MAC value with the initial reference of the tracked modes. 0.97 is the MAC value for the two 2SS mode references, but the MAC tendencies observed in Figure 46 c) and Figure 49 c) are opposite, reinforcing the thesis about the adaptative reference method loss in the tracking process.

The tracked damping ratios are generally below 4%, except for the modes 1SS and 1FA, where values of 15.7% are registered, as shown in Figure 48. Mode 1FA registers higher damping values, due to the aerodynamic damping contribution that increases with the wind speed. In the 1SS mode, certain points exhibit this tendency despite the smaller aerodynamic forces in this direction. This can be explained by considering the interconnected movements in the perpendicular directions. Note that this is also observed for the tracked modes with fixed reference, represented in Figure 45.

Table 2 - Automated Modal Tracking Results for February, considering an adaptative reference.

Mode	Success Rate (%)	$\bar{f}(Hz)$	$\Delta f(\%)$	f_{std}	$\overline{MAC}$	MAC_{std}
1SS	87.547	0.356	6.500	0.002	0.928	0.081
1FA	43.732	0.354	9.703	0.006	0.810	0.214
1SS*	19.075	1.335	14.327	0.045	0.796	0.133
2SS*	34.486	1.811	9.884	0.042	0.469	0.142
2FA	82.299	2.806	7.040	0.019	0.826	0.174
2SS	74.386	2.844	6.763	0.021	0.732	0.154
3FA	28.030	3.744	8.036	0.055	0.793	0.153
3SS	5.748	3.821	7.527	0.067	0.741	0.136
3SS*	64.640	3.845	10.880	0.065	0.797	0.121
4FA	35.027	4.324	7.663	0.057	0.656	0.265

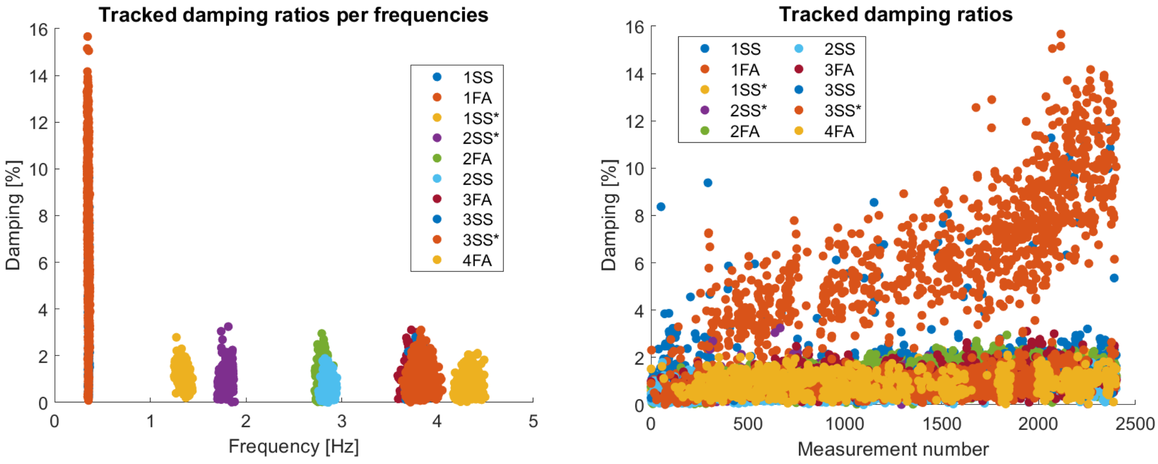

a) b)

Figure 48 - Damping evolution, considering adaptative reference: a) per frequency and b) per measurement, ordered by rotor speed.

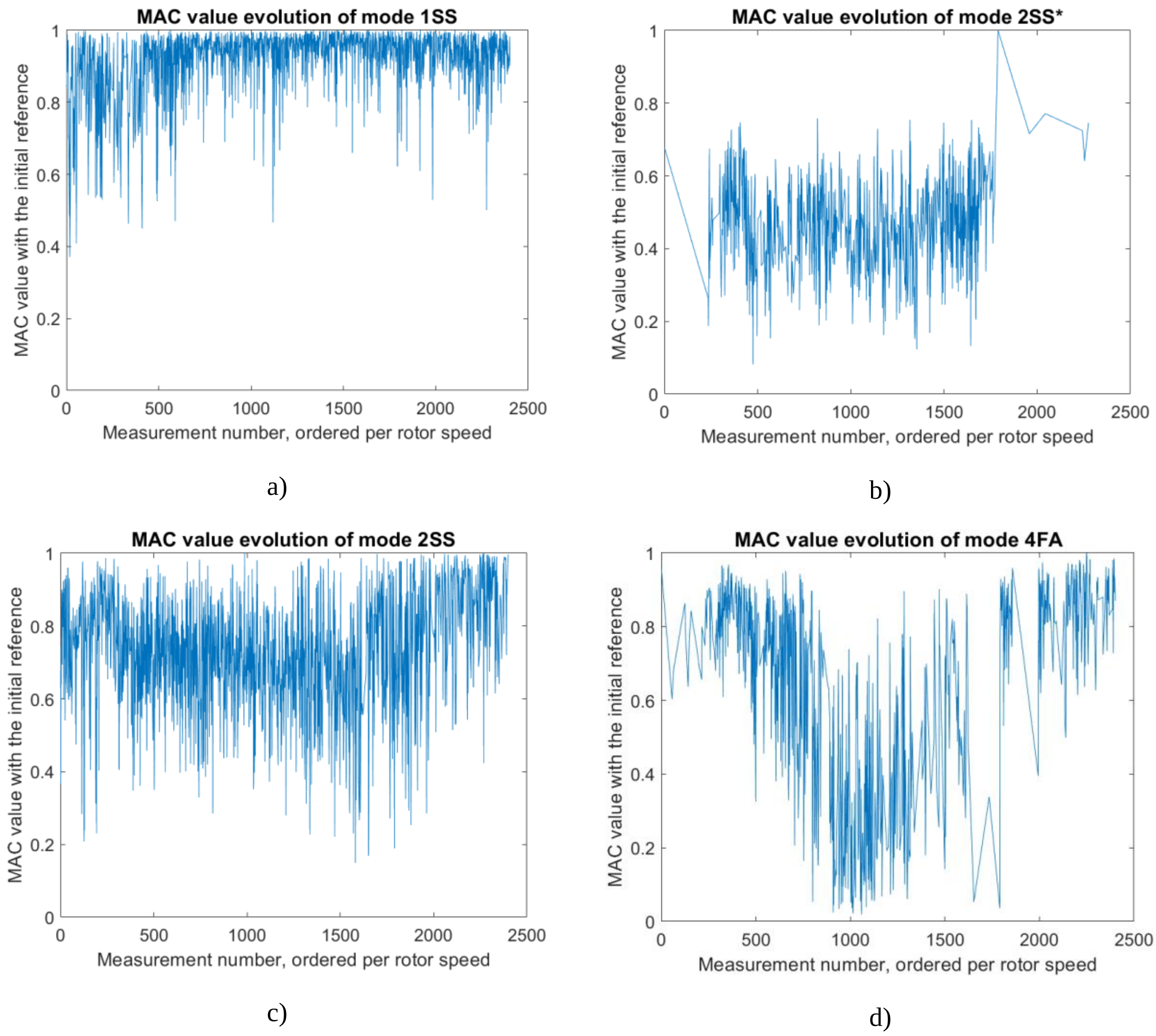

Figure 49 - MAC value evolution, considering adaptative reference, of modes: a) 1SS, b) 2SS*, c) 2SS and d) 4FA.

6.3. Impact of AMPS Methodology on Tracking Results

To ensure the tracking results are solely affected by the verification steps presented in the AMPS methodology, the tracking is performed considering only the DBSCAN step and with the fixed reference modes approach presented in subsection 5.2.1.

Figure 50 and Table 3 present, respectively, the AMT graph with frequencies for each measurement setup and the statistical results. Modes 1FA, 3SS, 3FA are represented in less than one fifth of the data sets, however mode 1SS is tracked in over 90%, which is in accordance with the previously presented results.

The frequency variation among all the tracked modes is within the range 6.5% to 7.0% and all the MAC values are above 0.8. Comparing the graph presented in Figure 46 with the ones in Figure 52 there are no significant changes to be noted, and these visual results are also present in results similarity between Table 1 and Table 3.

The results, while comparing the AMT with the verification steps or disregarding it, are clearly similar, which combined with the quality indicators stated, prove the robustness of the methodology addition. The sum of all the tracked modes is superior using the verification steps (Table 1) than when it is dismissed (Table 3) denoting an enhancement of the tracked results.

Figure 51 presents the tracked poles damping ratio, associated per tracked mode. The results obtained through this process are relatively similar to the ones registered in Figure 45, however in this case the 1SS damping ratio values are higher. This observation also enhances the positive impact of the verification steps in AMPS methodology.

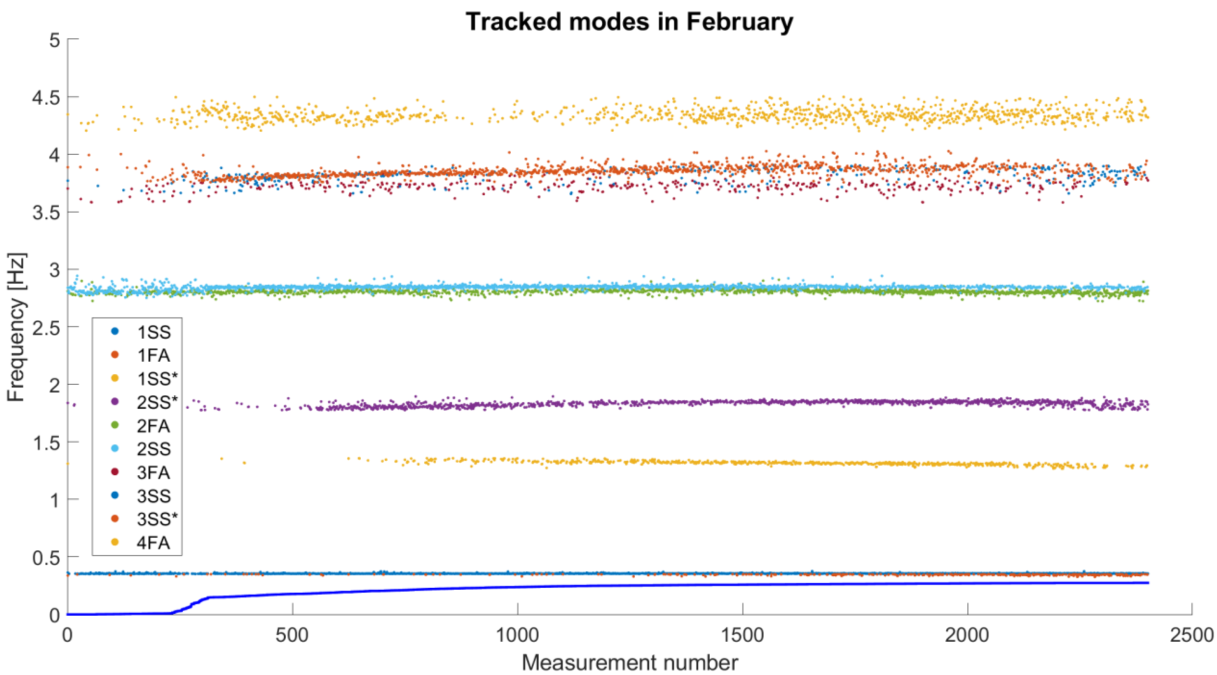

Figure 50 - Tracked modes in February 2014, with fixed reference and without the verification steps in AMPS, ordered for increasing rotor rotational speed.

Table 3 - Automated Modal Tracking Results for February, considering a fixed reference and without the verification steps in AMPS.

Mode	Success Rate (%)	$\bar{f}(Hz)$	$\Delta f(\%)$	f_{std}	$\overline{MAC}$	MAC_{std}
1SS	90.129	0.356	6.819	0.002	0.935	0.063
1FA	15.660	0.345	6.810	0.005	0.928	0.074
1SS*	31.320	1.316	6.885	0.017	0.826	0.070
2SS*	57.851	1.833	6.477	0.023	0.883	0.079
2FA	73.303	2.804	6.652	0.019	0.918	0.079
2SS	78.467	2.843	6.897	0.020	0.921	0.077
3FA	16.410	3.717	6.853	0.048	0.797	0.074
3SS	15.910	3.810	6.546	0.059	0.783	0.061
3SS*	52.436	3.855	7.008	0.047	0.841	0.075
4FA	47.813	4.342	6.938	0.056	0.862	0.079

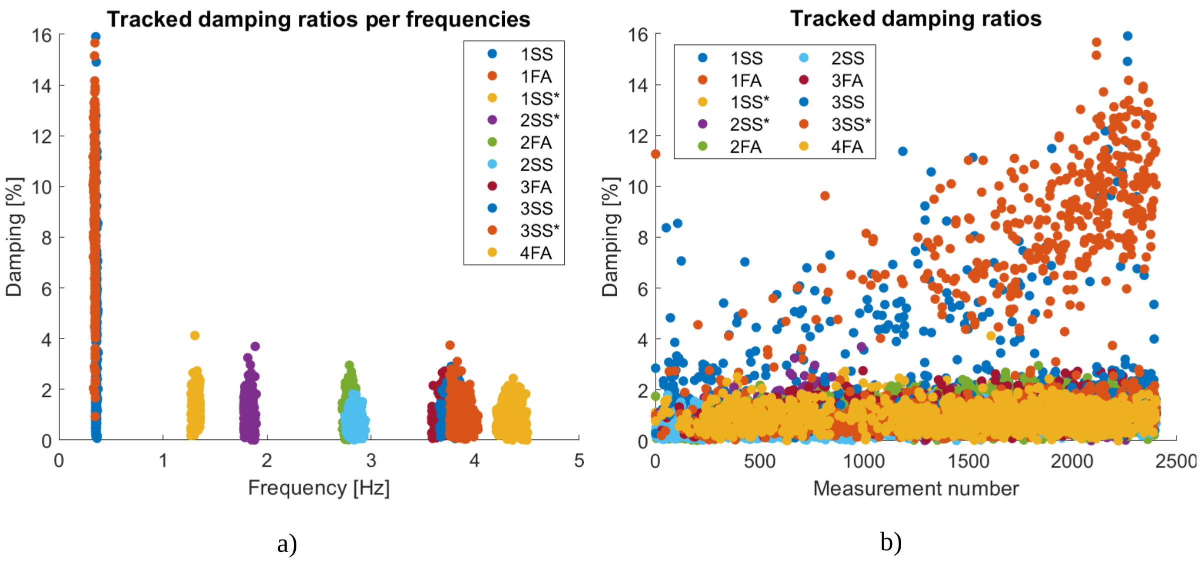

Figure 51 - Damping evolution, considering fixed reference and without the verification steps in AMPS: a) per frequency and b) per measurement, ordered by rotor speed.

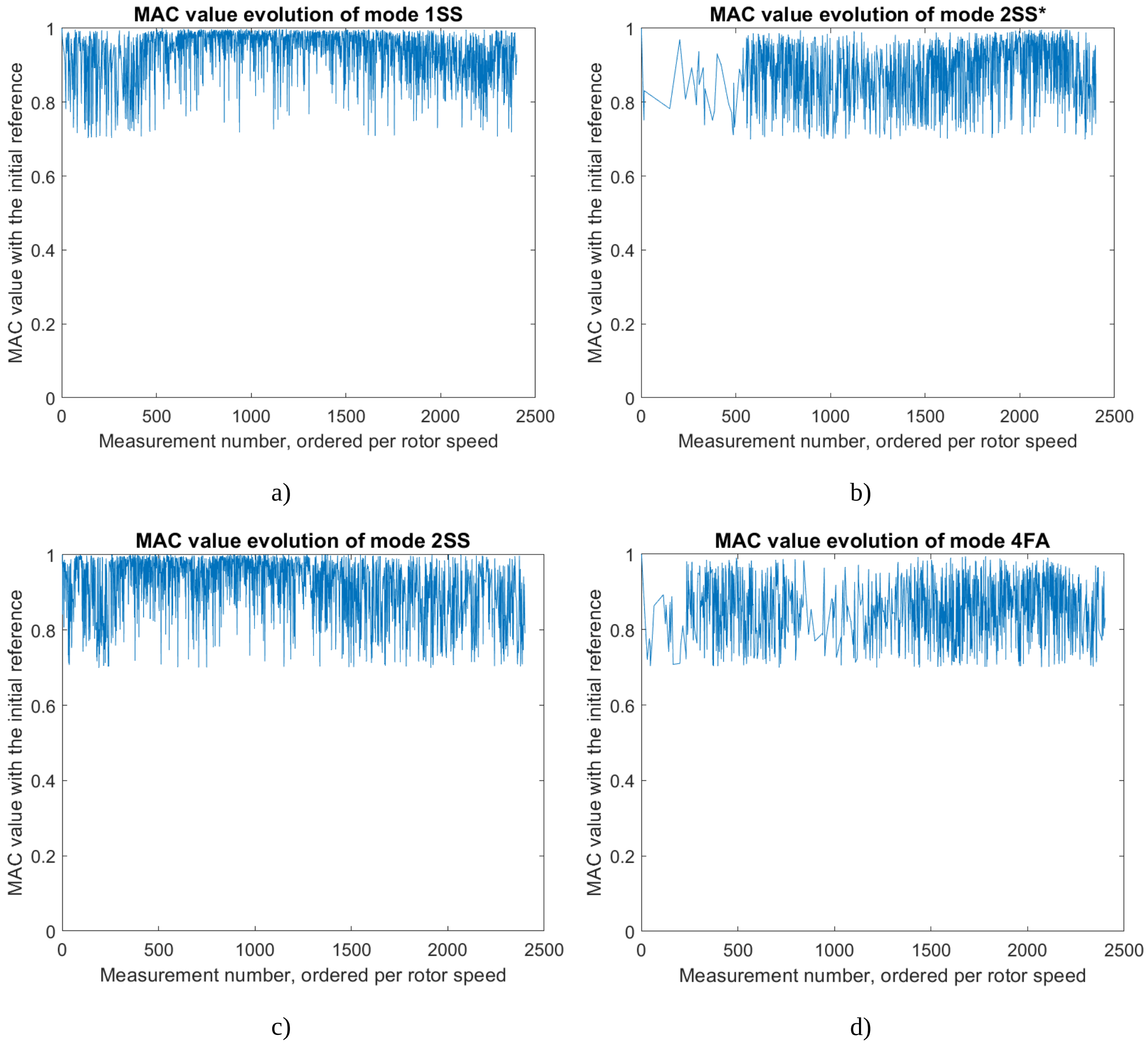

Figure 52 - MAC value evolution, considering fixed reference and without the verification steps in AMPS, of modes: a) 1SS, b) 2SS*, c) 2SS and d) 4FA.

6.4. Tracking Results for One-year Data

To accomplish the goal of this thesis, the AOMA methodology presented and developed in this project was applied to one-year data. A fixed reference was considered and the results are graphically presented in Figure 53.

The statistical data is in Table 4, from which the frequency variation close to 7% is observed for all the tracked modes, with a frequency standard deviation inferior to 5% to most of them, except for the high frequency modes: 3SS, 3SS* and 4FA. This is an expected outcome since the tracking procedure limits the frequency variation to a maximum percentage.

The average MAC value of each tracked pole with the associated reference mode is, generally, above 0.8 and their standard deviation bellow 9%. The mode 3SS registers the lowest average MAC value but has a smaller standard deviation, when compared to the other modes, what may indicate that the mode shape selected was not the most appropriate or that the procedure is tracking other modes, once the success rate associated is also reduced.

The MAC evolution over time registered for the modes 1SS, 2SS*, 2SS and 4FA show a mode shape variability with the rotor speed. For the mode 2SS* a tendency can be identified with the average MAC undulating in the allowed range (Figure 55 b)), indicating a mode shape modification with the rotor speed. Another note for this mode, is the experienced low tracking when the wind turbine is parked, once the frequency in this operating regime can diverge from the expected.

The damping results agree with the expectable growing damping ratio for the 1FA mode; however, this is also registered for the mode 1SS, which was also registered in previous analysis. Figure 54 b) indicates that after the rotor speed reaches its maximum (15.5 rpm) the damping increases enormously, which is related to the growing aerodynamic damping for increasing wind speeds.

The general results obtained indicate a good reliability in the tracked modes parameters.

The graph visual interpretation indicates that the tracking process is more fluctuant while the wind turbine is parked or idling, which is reinforced by the success rates obtained in this operating zone. Table 5 provides this information and only the modes 1SS and 2SS have been tracked in more than half of these setups, while the other vibration modes, except the 4FA, are identified in less than 10%. These results might be explained by the mode shapes variation with the rotor speed as reported by Oliveira in his work [20]. Additionally, the mode 2SS is the only with consistent success rates for both operational regimes analysed.

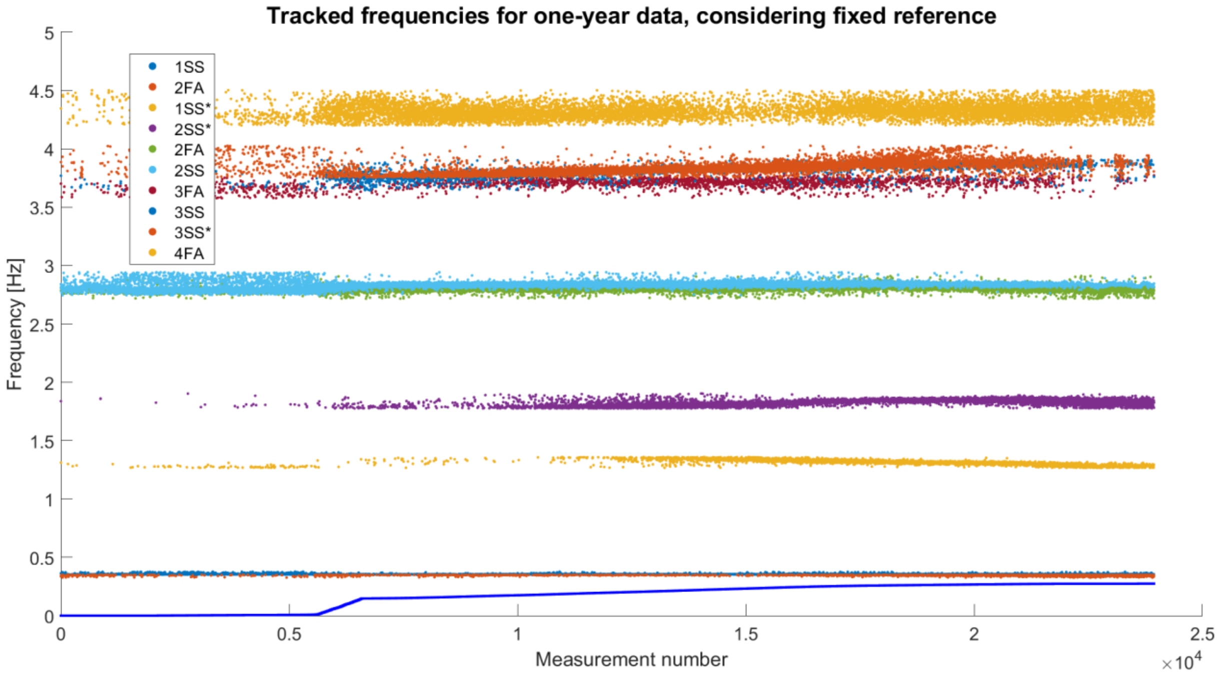

Figure 53 - Tracked modes in one-year measurements, with fixed reference, ordered for increasing rotor rotational speed.

Table 4 - Automated modal tracking results for one-year measurements, considering a fixed reference.

Mode	Success Rate (%)	$\bar{f}(Hz)$	$\Delta f(\%)$	f_{std}	$\overline{MAC}$	MAC_{std}
1SS	79.848	0.355	7.091	0.003	0.925	0.081
1FA	14.487	0.345	6.812	0.004	0.917	0.085
1SS*	20.628	1.313	6.998	0.020	0.819	0.058
2SS*	40.906	1.827	7.044	0.026	0.880	0.080
2FA	70.282	2.799	7.018	0.020	0.916	0.086
2SS	77.534	2.833	7.004	0.028	0.918	0.086
3FA	11.826	3.706	6.994	0.044	0.805	0.044
3SS	15.181	3.803	6.944	0.055	0.770	0.055
3SS*	37.990	3.841	7.083	0.051	0.838	0.067
4FA	48.880	4.328	7.035	0.062	0.871	0.082

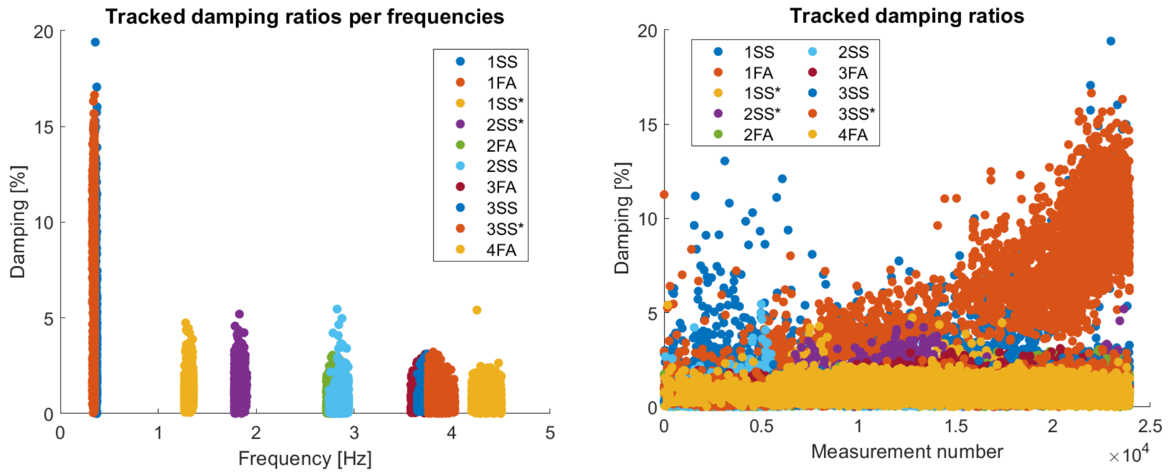

a) b)

Figure 54 - Damping evolution, for one-year measurements, considering fixed reference: a) per frequency and b) per measurement, ordered by rotor speed.

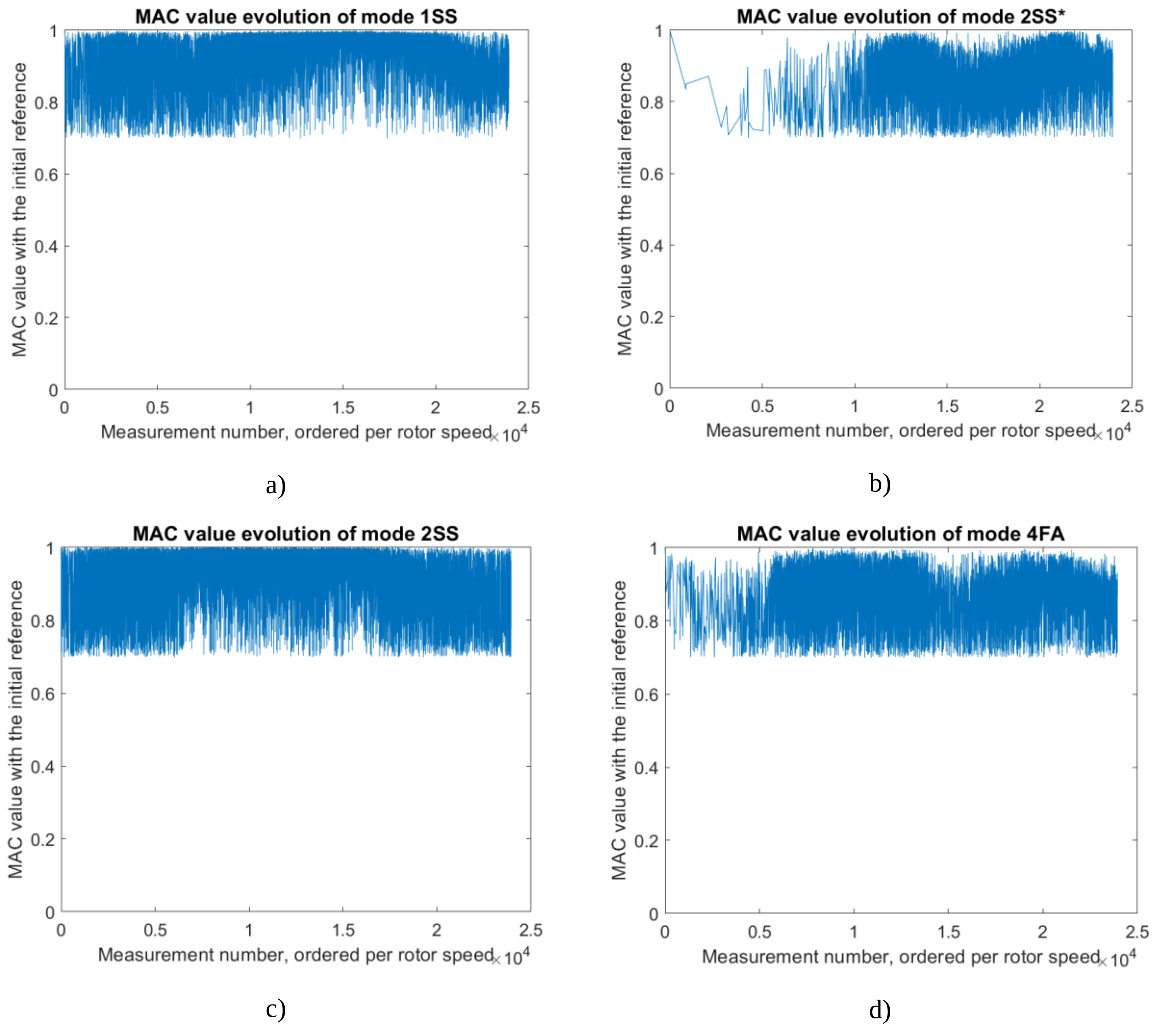

Figure 55 - MAC value evolution, for one-year measurements, considering fixed reference, of modes: a) 1SS, b) 2SS*, c) 2SS and d) 4FA.

Table 5 - AMT success rates considering 2 wind turbine operating conditions: a) parked or idling (rotor speed < 0.6 rpm) and b) rotor speed > 8.8 rpm.

Mode	Success Rate (%)	
	parked or idling (<0.6rpm)	rotor speed >8.8rpm
1SS	54.351	90.259
1FA	3.481	18.359
1SS*	1.489	27.934
2SS*	0.431	56.023
2FA	26.933	84.625
2SS	77.947	77.326
3FA	5.706	14.068
3SS	1.202	19.615
3SS*	7.106	48.897
4FA	7.949	61.697

7

CONCLUSIONS

7.1. ACHIEVEMENTS

The developed work intended to explore the potentialities associated with automated operational modal analysis (AOMA), to monitor the modal parameters of one wind turbine case study. An improvement in the algorithm to automated modal parameter selection was performed and different methodologies to do automated modal tracking were explored.

The initial motivation is related to the increasing potential of the wind turbine industry globally and to the need to monitor and access the structures characterization in an automated way, without requiring human interaction to do modal analysis. This is especially important to perform long-term monitoring, with reliable output modal parameters from the measured data.

The wind turbine structural behaviour was operationally and dynamically characterized. In the first phase, the structural elements and their operational conditions were described, including the cyclic vibration loading related with blades rotation. Therefore, the case study was introduced and the collected acceleration time-series data was used to access its real functioning and to pre-access modal information.

Then, the methodology utilized was improved, including the automated modal parameter selection (AMPS) method's modification, whose objective was to only merge clusters that clearly represent the same mode and maintain others separated. When comparing the results with and without the verification steps, the differences observed are negligible, but it has a positive impact on the tracked modes success rates and damping ratios.

For the automated modal tracking phase, the procedure was explained, and it was tested considering a fixed and an adaptative reference. This last methodology was implemented to analyse one month of collected data and it was verified that it is not a very generalizable process since the reference adaptation relies only in the frequency value and the wind turbine changes multiple times of operational regime, hence influencing its natural frequency. Thus, since the mode shapes are not assessed during this stage, it provided tracked modes with high MAC scarcity and often fluctuating to mode shapes diverging from the intended ones.

Regarding the damping tracking results, the mode 1SS is often associated with poles with higher damping than expected. These results can derive from the cross-frequency phenomenon with the 1FA mode, especially in setups for which the automated modal parameter selection method returned only one mode instead two for this pare o closely spaced frequencies.

The overall AMT results with fixed reference present good statistical indicators: frequency variation inferior to 7% and average MAC values above 0.8, despite the low success rate registered for some of the modes. Modes whose excitation depends on the rotor rotational movement register, generally, lower presence.

7.2. Future Work

The present work contributed to the automated operational modal analysis process, implemented to a wind turbine case study. However, there are some aspects that can be further developed and investigated to enhance the method applicability to this dynamic structural system:

- To develop an automated modal tracking methodology with adaptative references that introduces an indicator relating the mode shapes with the previous mode shapes tracked,
- To introduce damping as a modal parameter of relevance in the tracking procedure once the theory reveals its increase with increasing wind speeds for some modes.
- To improve the tracking procedure by defining a reference mode for each wind turbine operating regime, enhancing the reference adjustment to the operational conditions,
- To characterize the environmental and operational effects in the modal parameters,
- To increment, and equally distribute, the number of sensors along the tower height to assess with more reliability the tower accelerations and to enhance its modal characterization.

BIBLIOGRAPHY

[1] C. UAE, “Global Renewables and Energy Efficiency Pledge,” December 2023. [Online]. Available: https://www.cop28.com/en/global-renewables-and-energy-efficiency-pledge. [Accessed 9 June 2024].

[2] U. Nations, “Paris Agreement,” United Nations, Paris, 2015.

[3] GWEC, “Global Wind Report 2024,” Global Wind Energy Council, 2024.

[4] WindEurope, “Wind Energy in Europe,” Wind Europe, 2024.

[5] E. Comission, “European Wind Power Action Plan,” European Comission, Brussels, 2023.

[6] Reuters, “Portugal's renewable energy production hit new record in 2023,” 02 January 2024. [Online]. Available: https://www.reuters.com/business/energy/portugals-renewable-energy-production-hit-new-record-2023-2024-01-02/. [Accessed 09 June 2024].

[7] D.-G. f. C. o. Portugal, “National Energy Plan and Climate 2021-2030,” European Comision, Brussels, 2023.

[8] H. Ritchie, M. Roser and P. Rosado, “Renewable Energy,” *Our World in Data,* 2020.

[9] REN, “Renewable energy generation sets new record in 2023,” 02 January 2024. [Online]. Available: https://www.ren.pt/en-gb/media/news/renewable-energy-generation-sets-new-record-in-2023. [Accessed 09 June 2024].

[10] F. Pimenta, D. R. A. Ribeiro and F. Magalhães, “Modal properties of floating wind turbines: Analytical study and operational modal analysis of an utility-scale wind turbine,” *Engineering Structures 301,* p. 117367, 2024.

[11] R. Brinckner and P. H. Kirkegaard, “Special issue on Operational Modal Analysis,” *Mechanical Systems and Signal Processing,* p. 1209–1212, 2010.

[12] C. Devriendt, F. Magalhães, W. Weijtjens, G. De Sitter, Á. Cunha and P. Guillaume, “Structural health monitoring of offshore wind turbines using automated operational modal analysis,” *Structural Health Monitoring,* pp. 644-659, 2014.

[13] A. Tavares, E. Di Lorenzo, B. Cornelis, S. Manzato, B. Peeters, W. Desmet and K. Gryllias, “Automated modal analysis through Machine Learning: an industrial validation,” in *IMAC-XLI,* Austin, 2023.

[14] A. Tavares, E. Di Lorenzo, B. Cornelis, S. Manzato, B. Peeters and W. &. G. K. Desmet, “Automated modal analysis with density-based clustering: an industrial validation through jury testing,” *submitted* , 2024.

[15] F. Magalhaes, A. Cunha and E. Caetano, “Vibration based structural health monitoring of an arch bridge: From automated OMA to damage detection,” *Mechanical Systems and Signal Processing,* pp. 212-228, 2012.

[16] M. Mazzeo, D. De Domenico, G. Quaranta and R. Santoro, “Automatic modal identification of bridges based on free vibration response and variational mode decomposition technique,” *Engineering Structures 280,* p. 115665, 2023.

[17] B. Peeters and H. Van der Auweraer, “PolyMAX: a revolution in operational modal analysis,” in *Proceedings of the 1st International Operational Modal Analysis Conference*, Copenhagen, Denmark, 2005.

[18] B. Peeters and G. De Roeck, “Stochastic system identification for operational modal analysis: a review,” *J. Dyn. Sys., Meas., Control,* pp. 659-667, 2001.

[19] Y. Zhao, J. Pan, Z. Huang, Y. Miao, J. Jiang and Z. Wang, “Analysis of vibration monitoring data of an onshore wind turbine under different operational conditions,” *Engineering Structures,* vol. 205, p. 110071, 2020.

[20] G. Oliveira, “Vibration-based Strucutral Health Monitoring of Wind Turbines,” FEUP, Porto, Portugal, 2016.

[21] F. Magalhães, A. Cunha and E. Caetano, “Online automatic identification of the modal parameters of a long span arch bridge,” *Mechanical Systems and Signal Processing,* vol. 23(2), pp. 316-329, 2009.

[22] F. M. R. L. Magalhães, “Operational modal analysis for testing and monitoring of bridges and special structures,” Universidade do Porto, Porto, 2010.

[23] J. Teng, D. H. Tang, X. Zhang, W. H. Hu, S. Said and R. G. Rohrmann, “Automated modal analysis for tracking structural change during construction and operation phases.,” *Sensors* , vol. 19, p. 927, 2019.

[24] K. Kvåle and O. Øiseth, “Automated operational modal analysis of an end-supported pontoon bridge using covariance-driven stochastic subspace identification and a density-based hierarchical clustering algorithm,” in *Bridge maintenance, safety, management, life-cycle sustainability and innovations,* CRC Press, 2021, pp. 3041-3048.

[25] E. Reynders, J. Houbrechts and G. De Roeck, “Fully automated (operational) modal analysis,” *Mechanical systems and signal processing,* vol. 29, pp. 228-250, 2012.

[26] X. M. Yang, T. H. Yi, C. X. Qu, H. N. Li and H. Liu, “Automated eigensystem realization algorithm for operational modal identification of bridge structures,” *Journal of Aerospace Engineering,* p. 04018148, 2019.

[27] P. É. Charbonnel, “Fuzzy-driven strategy for fully automated modal analysis: Application to the SMART2013 shaking-table test campaign,” *Mechanical Systems and Signal Processing,* vol. 152, p. 107388, 2021.

[28] A. C. Dederichs, O. Øiseth, Ø. W. Petersen and K. A. Kvåle, “Comparison of automated operational modal analysis algorithms for long-span bridge applications,” in *Topics in Modal Analysis \& Parameter Identification, Volume 8: Proceedings of the 40th IMAC, A Conference and Exposition on Structural Dynamics 2022,* Springer, 2022, pp. 27-35.

[29] G. Oliveira, F. Magalhães, Á. Cunha and E. Caetano, “Continuous dynamic monitoring of an onshore wind turbine,” *Engineering Structures, 164,* pp. 22-39, 2018.

[30] A. Saisi, C. Gentile and M. Guidobaldi, “Post-earthquake continuous dynamic monitoring of the Gabbia Tower in Mantua, Italy,” *Construction and Building Materials,* vol. 81, no. Elsevier, pp. 101-112, 2015.

[31] C. Devriendt, W. Weijtjens, M. El-Kafafy and G. de Sitter, “Monitoring resonant frequencies and damping values of an offshore wind turbine in parked conditions,” in *IET Renewable Power Generation 8(4),* 2014.

[32] S. MacDonald, “OMG! What is OMA? Operational Modal Analysis - Siemens Community,” 10 July 2020. [Online]. Available: https://community.sw.siemens.com/s/article/OMG-What-is-OMA-Operating-Modal-Analysis. [Accessed 25 May 2024].

[33] P. Guillaume, P. Verboven, S. Vanlanduit, H. Van Der Auweraer and B. Peeters, “A poly-reference implementation of the least-squares complex frequency-domain estimator,” in *Proceedings of IMAC (Vol. 21, No. 01),* Kissimmee, FL, 2003.

[34] M. Aenlle López and R. Brincker, “Basic concepts of modal scaling,” in *8th IOMAC-International Operational Modal Analysis Conference,* Copenhagen, 2019.

[35] R. J. Allemang, “The modal assurance criterion: twenty years of use and abuse,” *Sound and Vibration, 37 (8),* pp. 14-23, 2003.

[36] M. Pastor, M. Binda and T. Harčarik, “Modal assurance criterion,” *Procedia Engineering,* pp. 543-548, 2012.

[37] M. Forrest, “Clustering For Fully Automated Modal Analysis,” KU Leuven, Leuven, 2022.

[38] E. Hau, Wind Turbines: Fundamentals, Technologies, Application, Economics, Krailling, Germany: Springer, 2006.

[39] C. Marquart, “University of Minnesota: Wind Over Morris,” July 2021. [Online]. Available: https://wcroc.cfans.umn.edu/research/renewable-energy/wind-over-morris. [Accessed 10 June 2024].

[40] E. Al-Ahmar, M. E. H. Benbouzid, Y. Amirat and S. B. Elghali, “DFIG-based wind turbine fault diagnosis using a specific discrete wavelet transform,” in *18th International Conference on Electrical Machines*, 2008.

[41] C. I. |. W. Power, “Wind Turbine Foundation: 5 Foundation Types Explained For Onshore Wind Turbine,” 09 May 2018. [Online]. Available: http://www.steelwindtower.com/wind-turbine-foundation-5-foundation-types-explained-for-onshore-wind-turbine/. [Accessed 10 June 2024].

[42] Goliathtechpiles, “A Wind Turbine Foundation System Using Helical / Screw Piles,” [Online]. Available: https://www.goliathtechpiles.com/application/helical-screw-piles-wind-turbines. [Accessed 10 June 2024].

[43] R. Clough and J. Penzien, Dynamics of Structures, Berkeley, USA: Computers & Structures, Inc., 1995.

[44] J. González-Hurtado, P. He, T. Newson, H. Hong, M. Postman and S. Molnar, “Field monitoring and analysis of an onshore wind turbine shallow foundation system,” *Dep,* 2017.

[45] I. E. Commission, “Design requirements for offshore wind turbines,” in *IEC 61400, 3,* 2006.

[46] J. Van der Tempel and D. P. Molenaar, “SOFT-SOFT, NOT HARD ENOUGH?,” in *Proceedings of the World Wind Energy Conference,* Berlim, 2002.

[47] Y. Zhang, C. Song and Z. Li, “Influence of Wind Turbine Structural Parameters on Wind Shear and Tower Shadow Effect,” *Energy Eng. J. Assoc. Energy Eng., 120(2),* pp. 501-510, 2023.

[48] B. Liu, X. Ma, J. Guo, H. Li, S. Jin, Y. Ma and W. Gong, “Estimating hub-height wind speed based on a machine learning algorithm: implications for wind energy assessment,” *Atmospheric Chemistry and Physics, 23(5),* pp. 3181-3193, 2023.

[49] M. Johnston, Static and modal analysis of wind turbine towers, Leicester, UK: De Montfort University, 1999.

[50] L. Chen, “Functionality investigation and expansion of 5kW wind turbine yaw and vibration sensors,” Murdoch University, 2017.

[51] J. Curt, M. Capaldo, F. Hild and S. Roux, “Modal analysis of a wind turbine tower by digital image correlation,” in *Journal of Physics: Conference Series 1618(2),* IOP Publishing, 2020, p. 022002.

[52] R. Barnes, “Wind Turbine Aerodynamics: Stall vs Pitch Regulation,” 09 June 2020. [Online]. Available: https://www.youtube.com/watch?v=Y5T5ZhJQr2o. [Accessed 10 June 2024].

[53] C. Cooney, R. Byrne, W. Lyons and F. O'Rourke, “Performance characterisation of a commercial-scale wind turbine operating in an urban environment, using real data,” *nergy for Sustainable Development,* vol. 36, pp. 44-54, 2017.

[54] J. Zhang, M. Cheng, Z. Chen and X. Fu, “Pitch angle control for variable speed wind turbines,” in *Third international conference on electric utility deregulation and restructuring and power technologies,* 2008.

[55] J. Lau, J. Lanslots and B. &. V. d. A. H. Peeters, “Automatic modal analysis. Reality or myth?,” *VDI BERICHTE,* p. 103, 2007.

[56] S. E. Project, “Spatial aliasing concept,” Stanford Exploration Project, 10 October 1997. [Online]. Available: https://sepwww.stanford.edu/sep/prof/iei/omk/paper_html/node13.html. [Accessed 14 June 2024].

[57] M. Civera, L. Sibille, L. Z. Fragonara and R. Ceravolo, “A DBSCAN-based automated operational modal analysis algorithm for bridge monitoring.,” *Measurement, 208,* p. 112451, 2023.

[58] K. Oukassou, S. El Mouhsine, A. El Hajjaji and B. Kharbouch, “Comparison of the power, lift and drag coefficients of wind turbine blade from aerodynamics characteristics of Naca0012 and Naca2412,” in *Procedia Manufacturing, 32,* 2019, pp. 983-990.

[59] N. J. Tarp-Johansen, L. Andersen, E. D. Christensen, C. Mørch, S. Frandsen and B. Kallesøe, “Comparing sources of damping of cross-wind motion,” in *European Offshore Wind 2009: Conference & Exhibition: 14-16 September,* Stockholm, Sweden, 2009.

[60] S. Vanlanduit, P. Verboven, P. Guillaume and J. Schoukens, “An automatic frequency domain modal parameter estimation algorithm,” *Journal of Sound and vibration, 265,* pp. 647-661, 2003.

[61] S. Yıldırım, “DBSCAN Clustering — Explained,” 22 April 2022. [Online]. Available: https://towardsdatascience.com/dbscan-clustering-explained-97556a2ad556. [Accessed 10 June 2024].

[62] B. Li, W. Liang, S. Yang and L. Zhang, “Automatic identification of modal parameters for high arch dams based on SSI incorporating SSA and K-means algorithm,” *Applied Soft Computing,* vol. 138, p. 110201, 2023.

[63] L. Sibille, M. Civera, L. Zanotti Fragonara and R. Ceravolo, “Automated Operational Modal Analysis of a Helicopter Blade with a Density-Based Cluster Algorithm,” *AIAA Journal,* vol. 61(3), pp. 1411-1427, 2023.